DETERMINATION OF CADMIUM BOUND TO WHEY PROTEINS BY LASER-INDUCED BREAKDOWN SPECTROSCOPY AT LOW PRESSURES

A Thesis Submitted to
the Graduate School of Engineering and Sciences of
İzmir Institute of Technology
in Partial Fulfillment of the Requirements for the Degree of

MASTER OF SCIENCE

in Chemistry

by
İlayda YAMAN

December 2023
İZMİR

We approve the thesis of **İlayda YAMAN**

Examining Committee Members:

Prof. Dr. Elif KAÇAR
Department of Physics, Kocaeli University

Asst. Prof. Dr. Enver TARHAN
Department of Physics, İzmir Institute of Technology

Prof. Dr. Şerife H. YALÇIN
Department of Chemistry, İzmir Institute of Technology

08 December 2023

Prof. Dr. Şerife H. YALÇIN
Supervisor, Department of Chemistry
İzmir Institute of Technology

Prof. Dr. Gülşah ŞANLI MOHAMED
Head of the Department of Chemistry

Prof. Dr. Mehtap Eanes
Head of the Graduate School of Engineering and Science

ACKNOWLEDGMENTS

I am deeply grateful to everyone who helped and supported me in the development and completion of my thesis.

First, I extend my heartfelt appreciation to my esteemed advisor, Prof. Dr. Şerife YALÇIN, for her guidance, support, and invaluable suggestions throughout the completion of this thesis study. I am deeply grateful to my advisor for giving me the opportunity to work with her, for devoting her time, sharing her valuable knowledge, and for constant encouragement.

I express my sincere gratitude to Prof. Dr. Elif KAÇAR and Asst. Prof. Dr. Enver TARHAN for readily accepting membership in my thesis committee. I appreciate their interest, assistance, and for sparing their valuable time.

Also, I would like to thank the Biological Mass Spectrometry and Proteomics Facility of İYTE, BMSPF, for providing cut-off filters and Assoc. Prof. Dr. Alper Arslanoğlu for providing BSA protein standards.

I wish to express my most special thanks to my mother, Nilüfer YAMAN, and my father, Sezgin YAMAN, who brought me to this day and stood by me under all circumstances. Without their support and understanding, it would not have been easy to complete this process successfully. I would also like to thank my sister Yasemin BAYRAK for her support and encouragement at every stage of my life. Also, I would like to thank Harun ERDOĞRUL for his support, interest, and for being with me in every aspect of my life.

With my deepest gratitude, I dedicate this work to my family.

ABSTRACT

DETERMINATION OF CADMIUM BOUND TO WHEY PROTEINS BY LASER-INDUCED BREAKDOWN SPECTROSCOPY AT LOW PRESSURES

In this thesis study, a dried-droplet LIBS methodology at reduced pressures for determining cadmium in aqueous media and in biological samples has been developed. With the advantage of the signal enhancement effect at reduced pressures, the optimum pressure for Cd detection was determined. Results were justified with the plasma images taken at different pressures. 100 mbar pressure was found as the optimum for most emission lines of Cd. To find the most suitable substrate onto which analyte droplets will be loaded, silicon wafer-based substrates of different coating types and coating thicknesses were studied. Among them, the c-Si substrate was found to show the highest signal enhancement for Cd detection. The performance of the methodology for quantitative analysis of Cd was shown by standard solutions and certified reference water samples. Calibration curves were constructed, and performance characteristics (limit of detection, accuracy, precision) were evaluated. Detection limits in absolute amounts of 6.8 pg and 1.05 pg were obtained at atmospheric and 100 mbar pressures, respectively. The application studies involve the determination of Cd bound to whey proteins. For this purpose, standard protein (BSA) and whey protein extracted from the milk were incubated in standard Cd solutions for several hours and filtered through cut-off filters via centrifugation. The unreacted cadmium in the filtrate and Cd-bound protein in fraction were analyzed separately.

It has been shown that dried-droplet LIBS at reduced pressures is a suitable methodology for identifying and determining Cd and Cd bound to proteins with a picogram amount of detection capability.

ÖZET

PEYNİRALTI SUYU PROTEİNLERİNE BAĞLI KADMİYUMUN LAZER OLUŞTURMALI PLAZMA SPEKTROSKOPİ İLE DÜŞÜK BASINÇLARDA BELİRLENMESİ

Bu tez çalışmasında, sulu ortamlarda ve biyolojik numunelerde kadmiyum tayini için düşük basınçlarda kuru-damla LIBS tekniğine dayalı bir metod geliştirilmiştir. Düşük basınçlarda sinyal iyileştirme etkisinin avantajı ile Cd tayini için optimum çevresel basınç koşulları belirlenmiştir. Sonuçlar farklı basınçlarda alınan plazma görüntüleri ile doğrulanmış, bir çok Cd emisyon bandı için optimum basınç 100 mbar olarak bulunmuştur. Analit damlacıklarının yükleneceği en uygun substratı bulmak için farklı kaplama tipi ve kaplama kalınlıklarına sahip silikon gofret bazlı substratlar üzerinde çalışılmıştır. Bunlar arasında c-Si substratının Cd tespiti için en yüksek sinyal artışı gösteren substrat olduğu belirlenmiştir. Metodolojinin kantitatif kadmiyum analizine yönelik performansı, standart çözeltiler ve sertifikalı referans su numuneleri ile gösterilmiştir. Kalibrasyon eğrileri oluşturulmuş ve performans özellikleri (tespit sınırı, doğruluk, kesinlik) değerlendirilmiştir. Atmosfer basıncında ve 100 mbar basınçta sırasıyla 6,8 pg ve 1,05 pg'lik mutlak miktarlarda tayin limitleri elde edilmiştir. Uygulama çalışmaları peynir altı suyu proteinlerine bağlı Cd belirlenmesini içermektedir. Bu amaçla sütten ekstrakte edilen standart protein (BSA) ve peynir altı suyu proteini, standart Cd solüsyonlarında birkaç saat bekletildikten sonra santrifüj yoluyla uygun filtrelerden süzülmüş, süzüntüdeki reaksiyona girmemiş kadmiyum ve fraksiyondaki Cd'ye bağlı protein ayrı ayrı analiz edilmiştir.

Tez kapsamında yapılan çalışmalarda, kuru-damla LIBS yöntemi ile düşük basınç koşullarında, Cd ve Cd-bağlı proteinlerin pikogram miktarında teşhis ve tayin edilebilirliği gösterilmiştir.

TABLE OF CONTENT

LIST OF FIGURES..…….…….…....viii

LIST OF TABLES……...……....xi

CHAPTER 1. INTRODUCTION……..….…...1

1.1 Laser-Induced Breakdown Spectroscopy (LIBS)……1

1.1.1 Theory…….2

1.2 Laser-Induced Plasma……..3

1.2.1 Effect of Ambient Atmosphere……4

1.3 Advantages and Disadvantages of the LIBS……...5

1.4 Instrumentation of LIBS……..6

1.4.1 Lasers…….…….……7

1.4.2 Optical Components…….……...9

1.4.3 Spectrographs and Detection System……...……10

1.5 Liquid Analysis by LIBS…….……..11

1.6. Cadmium Detection in Liquid Samples by LIBS…….……12

CHAPTER 2. BIOLOGICAL APPLICATION OF LIBS……..….14

2.1 Literature Studies…….….……14

2.2 Cadmium Binding Proteins…….……..16

2.3 Whey Proteins…….……..17

2.4 Aim of the Study…….……..19

CHAPTER 3. EXPERIMENTAL……...…..…..20

3.1 Experimental LIBS Set-Up……..……..20

3.2 Silicon Wafers……..……..21

3.3 Chemicals……..…….22

3.4 Methodology.……....……..……..23

3.4.1 Cadmium Binding to BSA….……..…….…...…….23

3.4.2 Whey Protein Isolation from Milk…..…..……24

3.4.3 Cadmium Binding to Whey Protein…....…….…….24

3.5 Dried Droplet Analysis..…….……..…..……...25

CHAPTER 4. RESULTS AND DISCUSSION…….....26
4.1 Optimization of the Experimental Conditions for Cd Detection…...26
4.1.1 The Effect of Substrate Type on Cd Signal Intensity…...…....28
4.1.2 Effect of Ambient Pressure on Signal Intensity…….....…...30
4.1.3 Detector Timing Parameters……...……..34
4.1.3.1 Delay Time……..34
4.1.3.2 Gate Width……..35
4.1.4 Effect of Laser Energy……..…….……...36
4.2 Quantitative Analysis of Cd in Aqueous Environments…….....…38
4.2.1 Calibration Studies…….……..…….38
4.2.2 Method Validation Experiments……..…….……40
4.3 Application of the Methodology to Real Sample Analysis….....40
4.3.1 Incubation Studies of Cd and Bovine Serum Albumin
(BSA) Standard……..……..……41
4.3.2 Incubation Studies of Cd and Whey Protein Extracted
From Milk……..……..44

CHAPTER 5. CONCLUSION……47

REFERENCES……48

LIST OF FIGURES

Figure **Page**

Figure 1.1. Schematic representation of the LIBS process……....2

Figure 1.2. (a) Laser-induced plasma plume. (b) Schematic illustration of laser-induced plasma plume…...……..3

Figure 1.3. Representation of periods of laser-induced plasma. (td: the delay time, tb: gate width)…..……4

Figure 1.4. A schematic representation of a typical LIBS set-up……..7

Figure 1.5. Schematic representation of laser source……7

Figure 1.6. a) Absorption and b) spontaneous emission mechanisms……...8

Figure 1.7. Stimulated emission mechanism……8

Figure 1.8. Schematic representation of flash lamp pumped solid state Nd:YAG laser...9

Figure 1.9. Diagram of (a) an echelle and (b) a Czerny-Turner spectrometer……10

Figure 3.1. Schematic representation of experimental LIBS set-up……21

Figure 3.2. Piece of p-type c-Si wafer (25x25mm) (a) before marking (b) after marking (c) after laser shot……..……21

Figure 3.3. a) 75 nm b) 300 nm c) 450 nm d) 1000 nm Si_3N_4 coated (e) 300 nm SiO_2 coated silicon wafers……...……22

Figure 3.4. Steps of BSA bound Cd analysis by dry droplet methodology. (a) Protein-Cd complex solution (b) unreacted Cd (c) Cd bound protein analysis ……..…….……23

Figure 3.5. Steps of whey protein isolation from milk…….…….24

Figure 3.6. Steps of dried droplet analysis. (a) marked c-Si wafer (b) c-Si wafer after loading 500 nL sample as droplets into the marked regions (c) c-Si wafer after drying the loaded droplets (d) craters formed after laser analysis of dried droplet…….....25

Figure 4.1. Representative LIBS spectra were obtained from 500 nL dried droplets of 1 ppm Cd with a laser pulse energy of 140 mJ, delay time of 500 ns, and gate width of 500 µs. Spectra was recorded with an echelle-type spectrometer…….....…27

Figure **Page**

Figure 4.2. LIBS spectra from 1 mg L-1 Cd solution, with Czerny-Turner spectrometer equipped with 3600 g/mm grating. Wavelength range of a) 212 nm to 218 nm, and b) 225 nm to 230 nm was used. Laser pulse energy of 140 mJ, Td =500 ns, Tg= 500 µs, 2 shot accumulation….……27

Figure 4.3. Comparison of the signal intensity (left) and signal-to-noise ratio (right) variation with Si-wafer substrates of different coatings and different coating thicknesses……..……29

Figure 4.4. Cd signal (at 226.5nm) variation with respect to ambient pressure. Cd signal for 1 mg.L^{-1} (ppm) Cd solution with Czerny-turner spectrometer of 3600 lines/mm grating……30

Figure 4.5. Effect of ambient pressure on different Cd emission lines for 2 ppm Cd solution dried on c-Si substrate. An echelle type spectrometer was used...…..…….….31

Figure 4.6. The variation in the LIBS emission signal of Cd for 1 ppm Cd solution at 226.5 nm and 228.8 nm with respect to ambient pressure and the plasma images at different ambient pressures…...……..33

Figure 4.7. Variation of LIBS signal intensity of Cd (II) at 226.5 nm with respect to the detector delay time (a) at atmospheric pressure and (b) at 100mbar……...……..…..35

Figure 4.8. Variation of LIBS signal intensity of Cd (II) at 226.5 nm with respect to the detector gate width (a) at atmospheric pressure and (b) at 100 mbar……..……36

Figure 4.9. LIBS signal intensity variation of 226.5 nm Cd (II) line with respect to laser pulse energy (a) at atmospheric pressure and (b) at 100 mbar……..……37

Figure 4.10. Calibration curves for Cd (II) 226.5 nm (a) at atmospheric pressure and (b) at 100 mbar reduced pressure conditions……..……39

Figure **Page**

Figure 4.11. Change in the unbound free Cd (II) signal intensity at 226.5 nm obtained as a result of bovine serum albumin and cadmium incubation at different incubation times (16, 24, and 48 hours) and molar concentration ratios (1:40 and 2:40 BSA: Cd)……..…….42

Figure 4.12. LIBS signal intensity variation with respect to incubation time for bound and unbound free-Cd to BSA with 1:40 molar ratio of BSA: Cd……...…...43

Figure 4.13. LIBS signal intensities of unreacted (free) Cd and the fraction containing Cd-bound protein equal the signal observed from unfiltered BSA-Cd complex solution after 26 hours of incubation at 37°C…….…..44

Figure 4.14. (a) UV-Vis spectra of whey protein extracted from milk by percentage in solution. (b) The relationship between the percentage of whey protein in a solution and the corresponding absorbance value.…45

Figure 4.15. LIBS signal intensities of unreacted (free) Cd and the fraction containing Cd-bound protein equal the signal observed from unfiltered whey-Cd complex solution……...……..45

Figure 4.16. Variation of 226.5 nm Cd(II) signal intensity with varying amounts of whey protein in the total solution……...…….46

Figure 4.17. Calibration curve for whey protein-Cd complex solution. The extracted whey protein was diluted to 1% in the final solution….....47

Figure 4.18. LIBS signal intensities of whey protein-Cd complex solution pre-concentration studies. The whey protein used was diluted as 1% in the final solution……..……....47

LIST OF TABLES

Table **Page**

Table 2.1. Major constituents of bovine whey……17

Table 4.1 Emission wavelengths of cadmium to zero energy level,
ionization energies, lower and upper-level configurations……..27

Table 4.2. Optimum experimental conditions for Cadmium (Cd)……..37

Table 4.3. Some concentration based LOD values from the literature for Cd.……...39

Table 4.4. Performance characteristics dried-droplet LIBS at reduced pressures…….41

CHAPTER 1

INTRODUCTION

1.1 Laser-Induced Breakdown Spectroscopy (LIBS)

Laser Induced Breakdown Spectroscopy (LIBS), also known as Laser Induced Plasma Spectroscopy (LIPS) and Laser Ablation Spectroscopy (LAS), is an optical atomic emission spectrochemical technique. Although there is yet to be a precise starting date for the modern version and application of LIBS, it is based on laser spectroscopy, which was proposed following the observation of laser-induced plasma in the 1960s (Cremers and Radziemski, 2006). The LIBS technique began to emerge in the 1980s with the detection of beryllium in filters using laser plasma, considered the pioneering work of Radziemski and Cremers (Cremers and Radziemski, 1985).

LIBS is a fast and powerful analytical technique for identifying and quantifying the elemental composition of various materials based on plasma formation at high temperatures because of focusing a high-intensity laser source in or on the sample surface. The plasma created by the laser ablates the material and creates a high-temperature environment where the atoms and ions are excited to emit characteristic spectral lines. The emitted light by atomic and ionic species is collected by a spectrometer and analyzed by a detector to identify the elements present in the sample and their concentrations. LIBS is a versatile technique used on various sample types, including solids, liquids, gases, and even biological tissues.

Various studies are being carried out using additional experimental techniques to increase the sensitivity of the LIBS technique and improve the signal intensity in experiments. Double-pulse LIBS (DP-LIBS) (Ahamer et al., 2018), LIBS coupled with laser-induced fluorescence (LIBS-LIF) (Elhamdaoui et al., 2022), surface-enhanced LIBS (SENLIBS) (Kaplan and Yalçın, 2022) and nanoparticle enhanced LIBS (NELIBS) (Khan et al., 2022) are the most widely used techniques.

Over the past few decades, LIBS has emerged as a valuable tool in numerous applications, such as metallurgy (Sun et al., 2015), environmental monitoring (Zhang et al., 2021), forensic analysis (Cicconi et al, 2020), pharmaceutical (Tiwari et al., 2017),

public safety (Burger et al., 2021), classification of polymer (Gajarska et al., 2021), cultural heritage and archaeology (Botto et al., 2019), biological samples (Janovszky et al., 2023) and many others.

1.1.1 Theory

LIBS is an analytical technique based on the principle that the analyte surface absorbs a laser pulse, and a small amount of material is removed, atomized, and ionized, creating plasma (Figure 1.1.). Plasma is a mixture of atoms, ions, and free electrons in the analyzed material. When the plasma cools, excited electrons and ions lose energy, return to their ground state, and emit light at characteristic wavelengths.

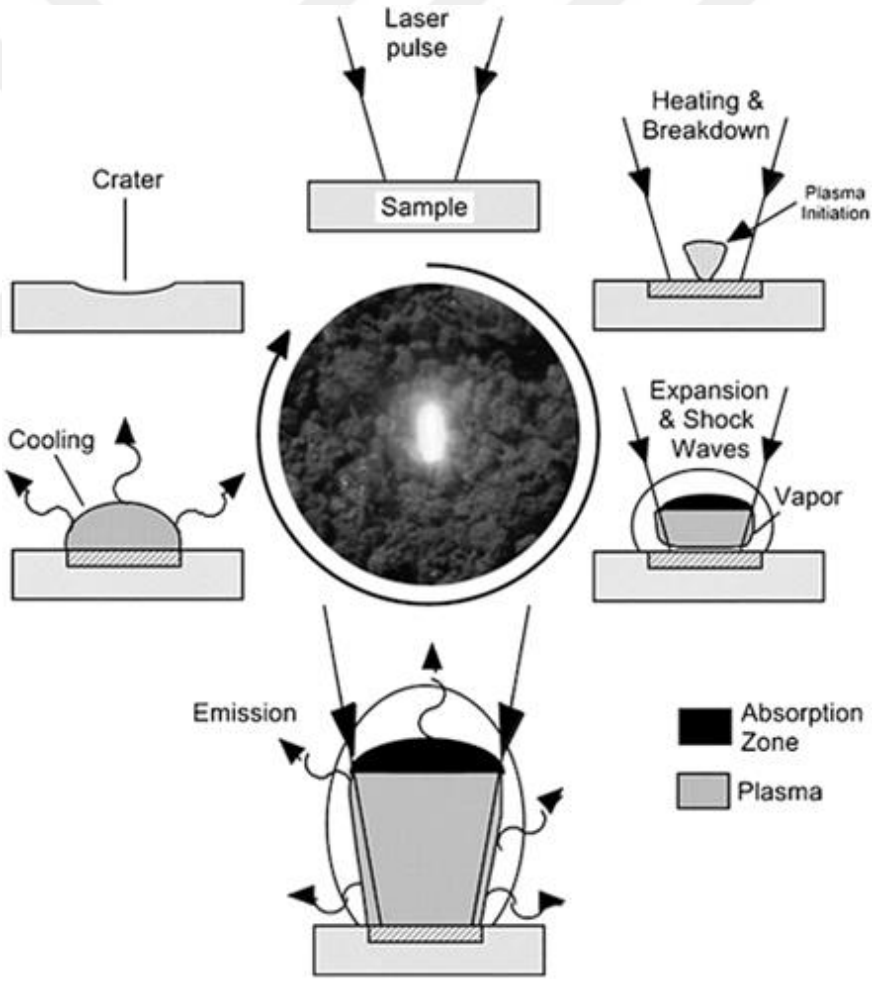

Figure 1.1. Schematic representation of the LIBS process (Cremers and Radziemski, 2006).

The light emitted by excited atoms and ions is collected with the help of a detection system consisting of an ICCD coupled with a spectrograph. The emission light of different wavelengths emitted by each element causes each element to have different emission lines.

1.2 Laser-Induced Plasma

The highly intense and energetic laser pulse delivers energy to the target surface, instantly melting, exciting, ionizing, and vaporizing the material into a plasma plume. Plasma is electrically neutral and consists of a combination of atoms, ions, and free electrons, and it has three main regions, as shown in Figure 1.2b. The core close to the target surface in plasma is the hottest and densest part; the material is mostly ionized due to high temperatures. In the middle region, ions and neutrals coexist due to ionization and recombination. The outermost region is relatively cold, where neutrals dominate and absorb radiation from the core and middle regions. Beyond these, a shock wave is produced by the explosive expansion of plasma. Also, the Knudsen layer exists near the target surface where the particles reach equilibrium velocity distribution (Chaudhary et al., 2016).

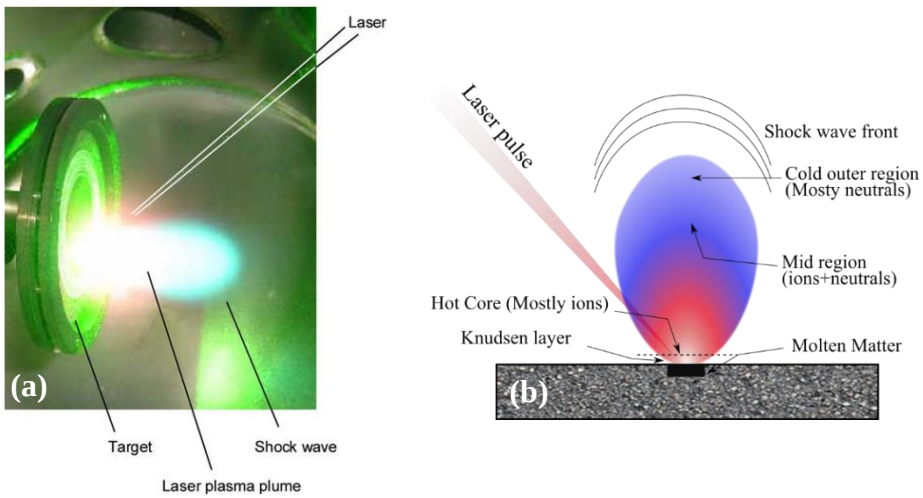

Figure 1.2. (a) Laser-induced plasma plume (Seto et al., 2005). (b) Schematic illustration of laser-induced plasma plume (Chaudhary et al., 2016).

LIBS plasmas are weakly ionized plasmas where the ratio of electrons to other species is less than 10%. The temporal period of a LIBS plasma initiated by a single laser pulse is shown in Figure 1.3. High ionization occurs initially, followed by the formation of neutral atoms and molecules. A continuous background is present during the process,

with spectral lines decaying slower than the background continuum. The continuum background results from bremsstrahlung and recombination. Bremsstrahlung occurs when electrons undergo acceleration or deceleration during collisions, while recombination involves the capture of a free electron into an ionic or atomic energy level (Cremers and Radziemski, 2006).

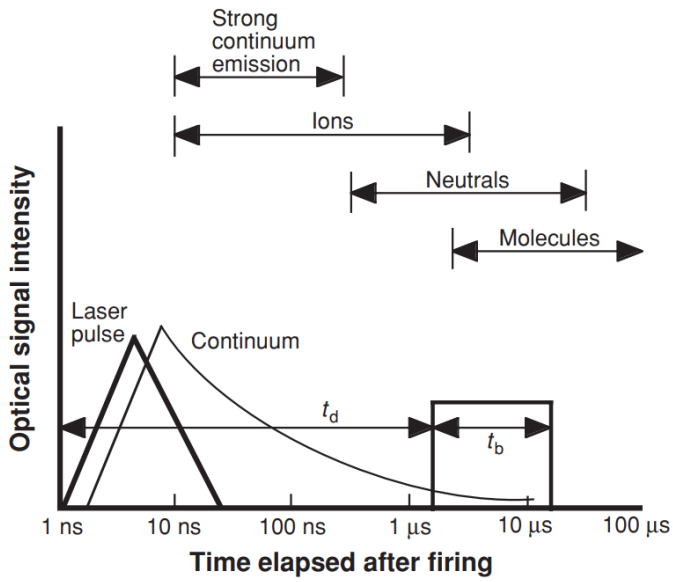

Figure 1.3. Representation of periods of laser-induced plasma. (t_d: the delay time, t_b: gate width) (Cremers and Radziemski, 2006).

1.2.1 Effect of Ambient Atmosphere

The laser-induced plasma is affected by the presence of gas around it and expands away from the target surface. The emission intensity is affected by gas type and ambient pressure. The shielding effect of the plasma plume reduces mass ablation. In a low-pressure environment, the plasma shielding effect decreases, resulting in more laser light reaching the sample and increasing ablation (Bashir et al., 2023).

Many studies report that LIBS studies performed at low pressures increase elemental signal intensity. In a low-pressure environment, collisions and interactions between plasma and gas molecules decrease. As a result of fewer collisions, the lifetime of ionic and neutral atoms increases. The increase in signal intensity can be attributed to the high number of particles in the plasma at a given time. In laser-induced plasma in a low-pressure environment, the signal-to-noise ratio (S/N) increases while the background level decreases.

Lowering the surrounding gas pressure provides several benefits, such as high spectral resolution, greater signal-to-noise ratio, increased spectral density, increased ablation, and more uniformly shaped ablation craters (Meng et al., 2020). Choi and coworkers (2016) conducted comprehensive studies on LIBS analysis of elements in various geological samples with pressures ranging from 0.01 to 760 Torr. Signal intensities decreased as the pressure decreased below 7 Torr, but S/N ratios increased due to reduced background emission. This shows that LIBS at low pressures is a promising tool for analyzing unknown samples and detecting traces of elements. Additionally, it has been shown that higher accuracy can be achieved under low-pressure conditions, and matrix effects can be reduced. Menegatti and coworkers (2019) analyzed cadmium in landfill leachate under controlled atmospheric and reduced pressure (100 Torr), and the detection limit of Cd increased by 5 times compared to atmospheric pressure. Bashir and coworkers (2023) investigated the surface and mechanical changes of copper and laser-assisted plasma and ablation parameters under controlled pressure (10 Torr-100 Torr). Crater depth, electron temperature, and electron number density increase up to a maximum of 60 Torr due to plasma confinement effects and increased collision frequency, while decreases between 60 and 100 Torr are due to the shielding effects of the plasma plume. Although no definitive atmospheric study exists, existing studies allow for improvements in LIBS spectra and detection limits by increasing signal intensity, resolution, and S/N ratio at reduced pressures (<760 Torr). In addition to ambient pressure optimization, other experimental parameters must be optimized for each application (Effenberger and Scott, 2010).

1.3 Advantages and Disadvantages of the LIBS

LIBS is a highly efficient and versatile method for analyzing the elemental composition of materials. Unlike other elemental analysis techniques, LIBS is non-destructive, requires no sample preparation, and can analyze any sample type, including solids, liquids, and gases. LIBS can also detect small amounts of a sample, even as tiny as a few micrometers. The technique provides real-time analysis, delivering rapid and highly accurate results. LIBS is a valuable tool in a wide range of applications that can detect almost all elements in the periodic table, including metals, non-metals, and metalloids. Moreover, the portability of LIBS technology makes it ideal for on-site

analysis in the field. In summary, LIBS is a reliable and efficient technique for elemental analysis that offers numerous benefits for researchers.

While LIBS presents numerous advantages, it also has some drawbacks. One such drawback is the need for high-energy laser pulses, which can be expensive and consume much power. Additionally, environmental factors such as humidity and temperature can significantly impact the accuracy and precision of the results. LIBS has relatively poor sensitivity and higher detection limits than other spectroscopy techniques like atomic absorption and inductively coupled plasma. Obtaining quantitative results with LIBS can be challenging due to variations in laser parameters, sample matrix effects, and the need for certified reference materials for certain elements. Furthermore, laser-induced plasma is formed on a very tiny size, and the spectral emission after laser ablation may not always represent the actual concentrations of species in the bulk samples. Nevertheless, despite these limitations, LIBS remains a valuable tool for analyzing a broad range of samples. Advancements in technology continue to enhance its efficacy while reducing its limitations.

1.4 Instrumentation of LIBS

A schematic diagram of the typical experimental setup for single-pulse LIBS is shown in Figure 1.4. The system consists of 3 main parts: a laser, optical materials as a focusing system, and a detection system. A highly energetic pulsed laser generates powerful pulses to form luminous plasma. The mirror that directs the laser pulse to the target surface and the focusing lens constitute the focusing system. The collection system consists of collection lenses and/or fiber optics, which collect the light emitted from the plasma and carry it to the detection system, which consists of a spectrometer and a detector that records the light.

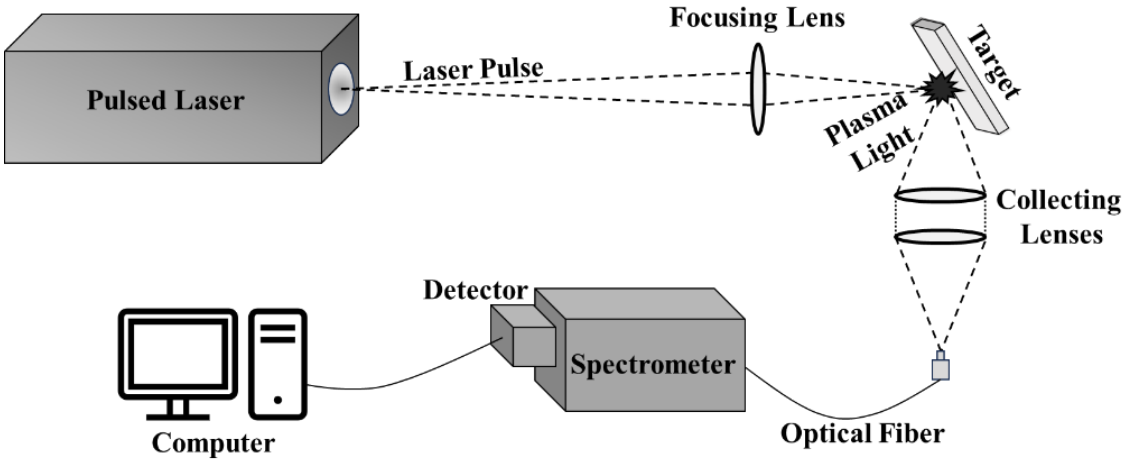

Figure 1.4. A schematic representation of a typical LIBS set-up.

1.4.1 Lasers

Lasers produce intense beams of coherent, directional, and monochromatic light. In short, lasers emit light through an optical amplification process based on the stimulated emission of electromagnetic radiation, the term derived from the acronym (L)ight (A)amplification by (S)timulated (E)mission of (R)adiation. A laser mainly consists of three main parts: an active (gain) medium to amplify the electromagnetic radiation, a pumping source to “pump” the active medium, and an optical resonator (cavity) to store a coherent electromagnetic field and enable the electromagnetic field to interact with the active medium.

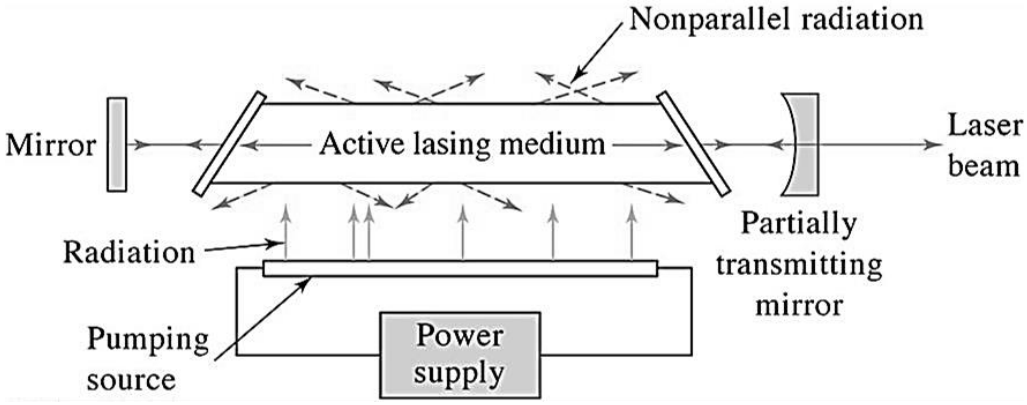

Figure 1.5. Schematic representation of laser source (Skoog et al., 2007).

The pumping source provides energy to the laser system. The pumping source excites the active medium to produce a population inversion. Then, spontaneous, and stimulated emission of photons occurs in the gain medium, leading to the optical gain or

amplification. In its simplest form, a resonator consists of two mirrors arranged so that light bounces back and forth before exiting the cavity as it passes through the gain medium each time. The light produced by spontaneous emission and coming from the medium is reflected into the medium by the mirrors and amplified by stimulated emission. While one of the two mirrors is a high reflector, the other is a partial reflector. The partially transparent one is called the output coupler because it emits the output laser beam.

Stimulated light emission is a crucial process required for a laser to work. Absorption, spontaneous, and stimulated emission are three interrelated energy conversion processes. Absorption is when an atom absorbs a photon of light; the energy causes an electron in an atom to go from a lower to an upper energy level (Figure 1.6a). Spontaneous emission is when an excited electron returns to a lower energy level without external energy and emits a photon (Figure 1.6b).

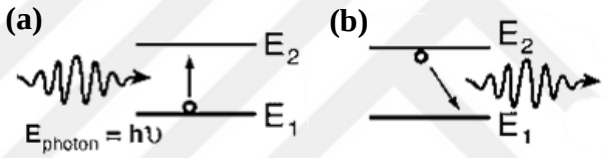

Figure 1.6. a) Absorption and b) spontaneous emission mechanisms.

If there is an electron in the already excited state and the energy of the incident photon (hν) is equal to the energy difference between the two states ($\Delta E = E_2 - E_1$), the electron can be stimulated to a lower level and produce a second photon with the same energy. The process where another photon acts as external energy is called stimulated emission (Figure 1.7).

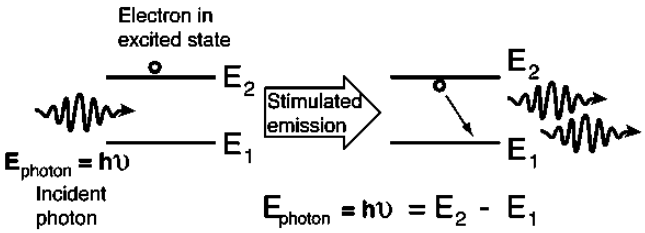

Figure 1.7. Stimulated emission mechanism.

The prerequisite for light amplification in lasers is population inversion, defined as a large population of electrons in the excited state. Lasers are defined as coherent light

sources because the photons produced by stimulated emission are in a definite phase relationship.

Depending on the gain medium, the pumping source can be flash lamps, arc lamps, another laser, chemical reactions, etc. So, various lasers rely on the pump sources and gain medium. Moreover, they can be listed as dye(liquid), gas, semiconductor, and solid-state lasers. Crystals and glasses can be used as a gain medium in solid-state lasers. Most LIBS systems use a Neodymium-doped Yttrium Aluminum Garnet (Nd:YAG) solid-state laser system pumped with a flash lamp, as shown in Figure 1.8. Nd:YAG solid-state lasers are widely used in LIBS measurements due to their high-power density and repetition rate. While Nd: YAG lasers operate at a wavelength of 1064 nm, the wavelength can be shifted by harmonic generation to 532 nm, 355 nm, and 266 nm.

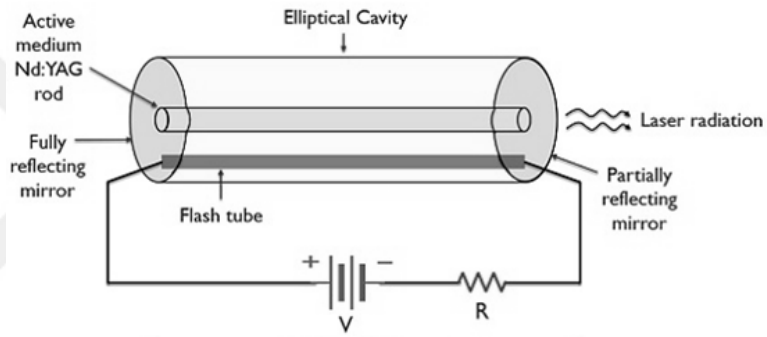

Figure 1.8. Schematic representation of flash lamp pumped to solid state Nd:YAG laser.

1.4.2 Optical Components

In LIBS, mirrors direct the laser pulse to the sample, while lenses or mirrors can focus laser pulses on the sample, and a light collection system consisting of lenses, mirrors, or fiber optics collects the spark light and carries it to the detection system. In the LIBS system, spherical optics are typically used to focus the laser beam, which allows the formation of circular dots and, therefore, symmetrical plasmas on the samples. The lens used must have maximum transmittance and transmit efficiently at the monitored wavelengths. Lenses with an anti-reflection coating are preferred because they minimize back reflections and maximize the energy at the target surface. Fiber optic cables are widely used with LIBS, as they simplify the collection of plasma light and are useful in applications where the detection system cannot be positioned close to the target (Cremers and Radziemski, 2006).

1.4.3 Spectrographs and Detection System

LIBS systems generally use a CCD array coupled with a spectrometer as a detection system. There are many different spectrometer configurations, the most common in LIBS analysis being the Czerny-Turner and Echelle spectrometers. A schematic description of Czerny-Turner and Echelle-type spectrometers is given in Figure 1.9. While the Czerny-Turner spectrometer relies on using a single dispersive element, the grating, the Echelle has two dispersive components, the grating and the prism (Musazzi et al., 2014).

The Czerny-Turner spectrometer operates for a small wavelength range because each spectral component leaves the grating by emitting in a different angular direction. Echelle spectrographs give higher spectral resolution and a broader wavelength range than the Czerny-Turner. However, Czerny-Turner has higher sensitivity, resulting in better detection limits for the LIBS system (Pořízka et al., 2016).

The LIBS system commonly uses the spectrometer with photomultiplier tubes (PMT), a photodiode (PDA), or a charge-coupled device (CCD) array for the detection and analysis of plasma lights. The PMT is a compact and sensitive detector that can be used for single wavelength detection when integrated with a monochromator. The PDA can be combined with a spectrograph to provide simultaneous detection in a specific spectral range, and it is possible to obtain one-dimensional spatial information about plasma lights. CCD detectors are preferred due to their high sensitivity, wide spectrum range, multi-element analyses, and two-dimensional analysis capabilities (Cremers and Radziemski, 2006; Musazzi et al., 2014).

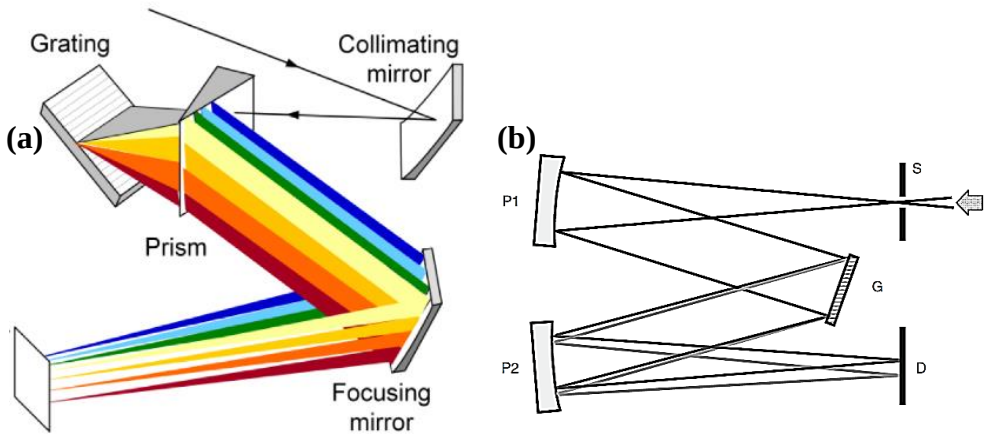

Figure 1.9. Diagram of (a) an echelle (Zhang et al., 2022) and (b) a Czerny-Turner spectrometer (Musazzi et al., 2014).

1.5 Liquid Analysis by LIBS

LIBS can perform multi-element analysis of all substances, such as solids, liquids, gases, and aerosols, with almost no preparation (Hussain et al., 2019). Although solid, liquid, and gas samples can be analyzed, liquid samples are relatively challenging to analyze due to some disadvantages. As a result of the interaction of the laser beam with the liquid sample, problems such as bubble formation in the liquid, splashing into the environment, and shock wave formation occur. As a result, poor signal quality and repeatability, reduced plasma emission, and high detection limits are observed (Zhang et al., 2021; Harun and Zainal., 2018). Therefore, liquid analysis performed with LIBS requires the application of some special methodologies or pretreatment steps before samples are analyzed directly.

Some experimental strategies are used in the literature to overcome the problems in liquids with LIBS. These include the double pulse LIBS (Xue et al., 2020), flowing jet liquids (Nakanishi et al., 2021), converting the liquid sample to the aerosol/gas phase (Aras et al., 2012), formation of volatile hydrides (Ünal and Yalcin, 2010) and liquid-to-solid conversion technique. Liquid-to-solid conversion covers the freezing sample into ice (Sobral et al., 2012), using adsorbent material like filter paper (Tan et al., 2012), sol-gel (Brouard et al., 2007), wood slice (Chen et al., 2010), hydrogel formation (You et al., 2023), immobilization on polymer membrane films (Lin et al., 2016) and dry droplet analysis on solid surfaces (Aras and Yalçın, 2016).

Dried droplet analysis with LIBS is a liquid analysis technique that directly analyzes dried and required amounts of liquid samples, eliminating the need for sample preparation and reducing contamination risk. It analyzes various biological, environmental, and industrial fluid samples. The dried droplet technique involves loading samples onto a suitable substrate, drying, and analyzing the light emitted by the plasma created by high-energy laser pulses.

In recent years, metallic and non-metallic substrates have been used in LIBS analyses with dried droplet methodology. Bae and coworkers (2015) devised a laser-patterned silicon wafer substrate for the analysis of K and Rb of a 15-µL droplet. Niu and coworkers (2018) deposited heavy metal solutions containing Ni, Cr, and Cd to a laser-pretreated aluminum substrate. Ma and coworkers (2019) studied four different substrates (zinc (Zn), magnesium alloy (Mg), nickel (Ni), and silicon (Si)) with different thermal

properties to analyze Cr and Pb elements in aqueous solution. Zn substrate was the best because of its lower boiling point, lower ablation threshold, and higher ablation quantity. Aras and Yalçın (2019) compared oxide-coated (SiO_2+Si) and nitride-coated silicon wafers (Si_3N_4+Si) with pure crystalline silicon wafer (c-Si) and Si_3N_4 showed better enhancement due to the low reflectivity and rapid dissipation of the heat into the matrix. Zhu and coworkers (2022) developed a superhydrophobic–super hydrophilic hybrid (SSH) substrate by coating polydimethylsiloxane and silicon dioxide nanoparticles on glass sequentially to suppress the coffee ring effect.

1.6 Cadmium Detection in Liquid Samples by LIBS

Cadmium is a toxic substance that is of concern due to its significant health risks and environmental impacts. Cadmium, a soft, silvery-white metal in the transition metal group, finds application in various industries such as paint, plastics, electronics, and batteries. However, it is considered a carcinogen in humans, and when it accumulates in the body, it causes kidney damage, lung cancer, and osteoporosis. Exposure occurs mainly through inhalation in occupational settings such as mining and smelting and can result from consuming contaminated food and water (Genchi et al., 2020).

In the literature, there are various studies on detecting cadmium in an aqueous solution and improving the LIBS methodology. In a recent study, a superhydrophobic-superhydrophilic hybrid substrate developed by sequentially coating PMDS and SiO_2 nanoparticles on glass was used as a substrate for dried droplet analysis for cadmium detection, and LOD value for Cd was calculated as 0.22 mg L^{-1} (Zhu et al., 2022). When a liquid-solid conversion method based on agarose films was used, the LOD value obtained for Cd was 0.011 mg L^{-1}(You et al., 2023). Another study enriched the filter paper with aqueous solutions to form a homogeneous sample layer on the metallic aluminum substrate surface. The detection limit was calculated as 0.165 mg L^{-1} with calibration curves (Xiu et al., 2020). In the study comparing pure crystalline, oxide-coated, and nitride-coated silicon wafers using the dried droplet technique, the LOD values obtained for Cd were 201, 151, and 124 ng mL^{-1}, respectively (Aras and Yalçın, 2019). In the study that used chelating resin to determine cadmium in drinking water, the calculated LOD was 3.6 μg L^{-1} (Tian et al., 2019). For the detection of Cd in solution, Ma et al. (2022) used the LIBS combined with electrodeposition and polished Al sheet was

used as the cathode in the system. The detection limit for Cd in a mixed solution is 4.86 μg L^{-1}. In another study, to improve the homogeneity and the adhesion force between the analytes and AuNPs, metal-chelate induced nanoparticle aggregation enhanced LIBS was proposed. For that purpose, the mixture was filtered with a membrane and analyzed directly, the detection limit for Cd was 4.6 ng mL^{-1} (Liu et al., 2020). In a study, Ruiz and coworkers (2019) combined dispersive micro solid-phase extraction with LIBS and used graphene oxide as an adsorbent for liquid analysis. The obtained LOD is 24 μg L^{-1} for Cd by using the DμSPE(GO)-LIBS methodology.

CHAPTER 2

BIOLOGICAL APPLICATIONS OF LIBS

Due to its prominent features, like speed and versatility, LIBS has been frequently used in biological research. Biological LIBS applications can be categorized into three groups. The first involves clinical samples analyses such as bones (Roldán et al., 2020), teeth (Alhasmi et al., 2015), gallstones and urinary stones (Jaswal and Singh, 2015; Mutlu et al., 2016), kidney stones (Oztoprak et al., 2012), nails and hair (Zhang et al., 2021), blood (Wang et al., 2023). The second one is the investigation of microorganisms that cause disease, such as bacteria (Mi et al., 2023; Arabi et al., 2023), fungi, molds, and yeasts (Singh et al., 2018). The third group of biological LIBS applications is based on the method development studies for determining important elements in biological matrices in trace amounts like phosphorous (Aras and Yalcin, 2014) and platin (Kaya, 2015) bound proteins.

2.1 Literature Studies

In a study in which cancerous and normal colon samples were analyzed by LIBS, carcinogenic heavy metals such as Pb, Cr, and Hg were found in malignant colon tissues. ICO-AES confirmed the results obtained, concluding that LIBS is suitable for distinguishing malignant and normal tissues (Gondal et al., 2020). Zhang and coworkers (2021) used a calibration-free LIBS (CF-LIBS) technique that does not require standard samples to obtain direct spectra of human biomarker hair and nails. In the obtained spectra, the intensity of the C, H, and O lines was more intense due to the greater ablation in the nails. Since many mineral elements in the human body are essential in biochemical processes, Ca/Na and Mg/Na content ratios in hair and nail samples were quantified. The results obtained were compared with the ICP-OES results, and it was determined that the relative error was less than 10%. In the study to evaluate the suitability of LIBS in the evaluation of skin cancer, typical skin tumors such as malignant melanoma, squamous cell carcinoma, basal cell carcinoma, and hemangioma were used. 3D elemental imaging

of Mg, Ca, Na, and K elements provided the element distribution in the tissue (Kiss et al., 2021).

Since liquid analyses were performed within the scope of this study, the focus was on liquid biological samples, and Wang et al. (2023) used the LIBS technique to determine electrolyte elements in human blood plasma. However, it has been combined with the surface-enhanced laser-induced breakdown spectroscopy (SENLIBS) gel film method to avoid the negative effects such as splashing, surface rippling, and plasma quenching that may occur in the blood sample when interacting with the laser and to increase the detection sensitivity. Blood plasma samples were deposited on metal substrates, naturally coagulated, and converted into jel film form for LIBS detection. It was observed that signal intensities collected from gel blood plasma increased 8.19 and 5.38 times compared to direct analysis for Na and K, respectively.

Chen et al. (2018) analyzed whole blood samples with LIBS to distinguish lymphoma from healthy ones and examined the results using chemometric methods. The collected whole blood samples were deposited and dried on filter papers, and 16 atomic and ionic emission lines such as Ca, Fe, Mg, K, and Na were selected. LIBS results combined with chemometric methods demonstrate that the technique can be used rapidly and accurately for detecting and discriminating human malignancies.

In the LIBS study conducted for the rapid detection of SARS-CoV-2 in plasma, it was observed that blood plasma taken from positive and negative SARS-CoV-2 donors was distinguished with up to 95% accuracy through elemental fingerprints containing elements such as Mg, Na, Ca, and CN. Blood plasma samples were placed on pure Si wafers during the experiments, and then the deposited blood plasma samples were dried (Berlo et al., 2022).

Markushin et al. (2015) used fs-LIBS and performed a multi-element analysis to detect the ovarian cancer biomarker (CA125) in human blood plasma. This study tagged non-fluorescent magnetic (Fe_3O_4) and non-magnetic (TiO_2) metal microparticles with specific monoclonal antibodies. Tag-LIBS assay was developed, and CA-125 detection was achieved with this method.

Aras and Yalçın (2014) worked on the suitability of the LIBS method for separating phosphorylated and non-phosphorylated proteins. Phosphorus-containing proteins such as casein and ovalbumin were separated by the SDS-PAGE method, stained, and dried, and then the protein bands were analyzed by LIBS. The applicability of LIBS

analysis after SDS-PAGE separation for the determination of phosphorous in protein samples was shown.

Kaya (2015) worked with standard proteins (human serum albumin, human apo transferrin, horse heart myoglobin) and proteins extracted from HeLa cancer cells to detect cisplatin-binding proteins in gel spots. In the study, proteins were incubated with cis-platin solution followed by non-reducing SDS-PAGE separation. After drying, the protein spots on the gel were analyzed by LIBS by monitoring the Pt emission lines. This study has shown the possibility of identification of Pt-binding proteins by LIBS after electrophoretic gel separation.

2.2 Cadmium Binding Proteins

Cadmium exhibits a variety of interactions with proteins, mainly through covalent binding with cysteine and other amino acids. This binding can lead to the breakdown of peptide bonds and, ultimately, inactivation or misfolding of the protein (Tamás et al., 2018). It is essential to know that the interaction of cadmium with proteins can trigger harmful consequences due to its toxicity (Rahimzadeh et al., 2017). Specific proteins containing thiol molecules can bind with Cd^{2+}. Besides low molecular-weight proteins like metallothionein, high molecular-weight proteins like albumin, transferrin, and α2-macroglobulin can bind with Cd (Kurowska and Bal, 2010; Fels et al., 2019).

Serum albumin can bind to heavy metals such as cadmium due to its cysteine residues, helping transport and detoxify them in the body. Liu and coworkers (2014) studied the binding mechanism of the Cd(II)-human serum albumin (HSA) complex and comprehensively investigated the effect of Cd(II) on the conformational stability and structural state of HSA. XPS analysis confirmed the direct interaction between polypeptide C, N, and O atoms of HSA and Cd(II). Fluorescence results showed a static quenching mechanism. Thermodynamic analysis and molecular docking revealed electrostatic interactions with negatively charged amino acids. FTIR analysis showed that increasing Cd(II) decreased α-helix and increased random coil structures in HSA. Cheng and coworkers (2022) investigated the interaction of Cd^{2+} and BSA in the absence and presence of chlorogenic acid (CGA), caffeic acid (CA), and phloretic acid (HPPA) with a surface plasmon resonance (SPR)-based analysis strategy. They observed that the presence of CGA, CA, and HPPA decreased the binding affinity of BSA with Cd^{2+} and

its structural changes. Hazra and coworkers (2017) synthesized a luminescent tetra-coordinated cadmium (II) complex and investigated the interactions of this complex towards BSA and HSA using spectroscopic techniques. Thermodynamic parameters showed that hydrophobic forces play an important role in the binding reaction, and the process is endothermic. Additionally, the biological significance of this study is emphasized, as albumin acts as an endogenous carrier for the complex in the body.

Within the scope of this thesis, cadmium bound to whey proteins was determined. In the study, Grassi et al. (2023) investigated the distribution of Pb and Cd added to milk in fat, casein and whey fractions by ICP-QMS. More than 94% of the heavy metals added to milk samples were found in skim milk, and the results showed that 1.97% of Pb and 3.67% of Cd were associated with the whey fraction.

2.3 Whey Proteins

Milk proteins consist of two groups: casein and serum proteins. About 20% of bovine milk protein is called serum (whey) proteins, which are soluble in milk serum at pH 4.6. Whey is the liquid that remains after milk is curdled or strained, and cheese whey is the most abundant commercially available whey product. Major whey proteins include β-lactoglobulin, α-lactalbumin, serum albumin, and immunoglobulins (Kilara and Vaghela, 2018; Guo and Wang, 2016).

Table 2.1. Major constituents of bovine whey.

Constituent	β-Lactoglobulin	α-Lactalbumin	Immunoglobulins (Predominantly IgG1)	Serum albumin	Lactoferrin
Concentration ($g\ L^{-1}$)	2.0-4.0	0.6-1.7	0.3-0.6	0.4	0.02-0.1
Molecular Weight	18.300	14.200	150.000-900.000	66.000	78.000

While β-Lactoglobulin is not present in human milk, it accounts for approximately 50% and 10% of the whey proteins and total proteins in bovine milk, respectively. Bovine β-Lactoglobulin consists of 162 amino acid residues per monomer and has a molecular weight of 18.3 kDa. It contains two disulfide bonds and one free cysteine group. While disulfide bonds prevent structural integrity from being damaged during hydrolysis and

heat treatment, the cysteine group is a binding site for d-block metal ions such as Fe^{2+}, Fe^{3+}, Cu^{2+}, etc. (Rozdik et al., 2020; O'Mahony and Fox, 2014).

α-Lactalbumin is the major protein, accounting for approximately 22% of the total protein of human milk. Consisting of 123 amino acids, α-Lactalbumin constitutes about 3.5% and 20% of the total and whey protein in bovine milk, respectively. α-Lactalbumin has four disulfide bonds between cysteine residues to provide stabilization. It has a metal affinity to ions of s-block elements, such as Mg^{2+}, and transition metal ions, such as Zn^{2+}. While it has a single strong Ca^{2+} binding site that can bind Mg^{2+}, Mn^{2+}, Na^{+}, K^{+}, and some other metal cations, it has several different Zn^{2+} binding sites. While the binding of metal ions, especially Ca^{2+} ions, increases the stability of the protein, the binding of Zn^{2+} to the calcium-bound protein reduces stability and causes aggregation. (Rozdik et al., 2020; O'Mahony et al., 2014; Permyakov, 2020).

Immunoglobulins account for nearly 10%-15% of human and bovine milk whey proteins. There are three basic classes of immunoglobulins (IG) as IG_G, IG_A, and IG_M. IG_A is the major IG in human milk and colostrum, it is also found in bovine milk, but IG_G accounts for ~80% (w/w) of all IG in bovine whey. (Madureira et al., 2007; Fenelon et al., 2019).

The bovine whey protein fraction includes lactoferrin between 0.02 and 0.1 g/L (Leischner et al., 2021). Bovine lactoferrin is the main iron-binding protein in milk. Depending on whether it binds iron (III), it can exist in two forms: apo-lactoferrin (without iron) and holo-lactoferrin (with two Fe^{3+} bonds). Although with lower affinity, it can bind other ions, such as Al^{3+}, Mn^{3+}, Cu^{2+}, and Zn^{2+} (Rodzik et al., 2020).

Since serum albumin in milk has similar properties to that in blood, it is thought that it cannot be synthesized in the mammary gland and instead appears in milk due to passive leakage from the bloodstream and maternal circulation. Bovine serum albumin (BSA) contains 582 amino acid residues and has 17 intermolecular disulfide bridges. Many ligands, including fatty acids and trace elements, are known to bind to serum albumin in the blood. Similarly, copper and zinc have also been linked to serum albumin found in milk. (Madureira et al., 2007; Fenelon et al., 2019).

2.4 Aim of the Study

This thesis study aims to improve cadmium detection in aqueous solutions and biological environments by taking advantage of the LIBS signal enhancement effect at low pressure conditions. For that purpose, the most suitable non-metallic substrate was selected. Images of laser-induced plasma at different pressures were taken with the use of a Czerny-Turner type spectrograph coupled with ICCD, and the most appropriate ambient pressure for Cd detection in our system was determined with an emphasis on an increase in signal intensity. The ability of the methodology to quantitatively analyze Cd was demonstrated using standard solutions and certified reference water samples. Calibration curves were generated, and performance characteristics such as limit of detection, accuracy, and precision were evaluated.

Application studies of this methodology aim to determine the amount of Cd bound to whey proteins. Both standard protein solution (BSA) and whey protein isolated from bovine milk were mixed with standard Cd solutions and incubated under appropriate temperature, time, and pH conditions to form cadmium-bound proteins. The mixture was then filtered by centrifugation with cut-off filters, and the unreacted cadmium in the filtrate and the Cd-bound protein in the fraction were separated. LIBS measurements of unreacted Cd, Cd-bound protein, and BSA-Cd complex solution were performed separately and evaluated. Cd element bound to specific proteins were quantified via dried droplet LIBS methodology.

CHAPTER 3

EXPERIMENTAL

3.1 Experimental LIBS Set-Up

The LIBS system used in this thesis study consists of four main parts, including a laser source, optical materials, a vacuum chamber, and detection systems. In the LIBS system, a second harmonic 532 nm wavelength Q-switched Neodymium-doped Yttrium Aluminum Garnet (Nd:YAG) laser (Quanta-Ray Lab-170, Spectra-Physics, California-USA) operating at 10 ns duration and 10 Hz frequency was used for plasma formation. The pulse energy of the laser beam was measured with a power meter (PE50BB-DIF-V2, Nova II, Ophir). The laser beam emerging from the laser source is reflected and directed by 532 nm reflective mirrors (1'' OD, coated, 532 nm reflective, New Focus), and the laser beam is focused on the sample surface by a plano-convex lens with a focal length of 35 cm. To transmit the plasma emission occurring on the target material to the entrance slit of the spectrograph (a Horiba iHR 320 spectrometer equipped with an ICCD (iStar334T, Andor Inc.)), the plasma is collected by two plano-convex lenses (2 " OD, 532 nm reflective, plano-convex lens, New Focus) and focused on the slit.

For low-pressure LIBS experiments, a vacuum chamber with an octagonal structure made of stainless steel was used. The arms of the chamber were used for purposes such as focusing the laser beam on the material, controlling the position of the laser beam on the target with the camera and monitor system (Honeywell, HMM9/HMM9X), collecting the emitted beam and sending it to the spectrograph, providing a low-pressure environment with the vacuum pump (Varian TriScroll 600 Inverter Pump), controlling the pressure values with vacuum gauge (Agilent Varian AGC-100) and for the motion of the motorized XY-translational stage (New Focus, Darmstad-Germany).

The schematic diagram of the experimental LIBS setup is shown in Figure 3.1. In the figure, M1, M2, and M3 are reflective mirrors, and ICCD is an inductively charge-coupled detector.

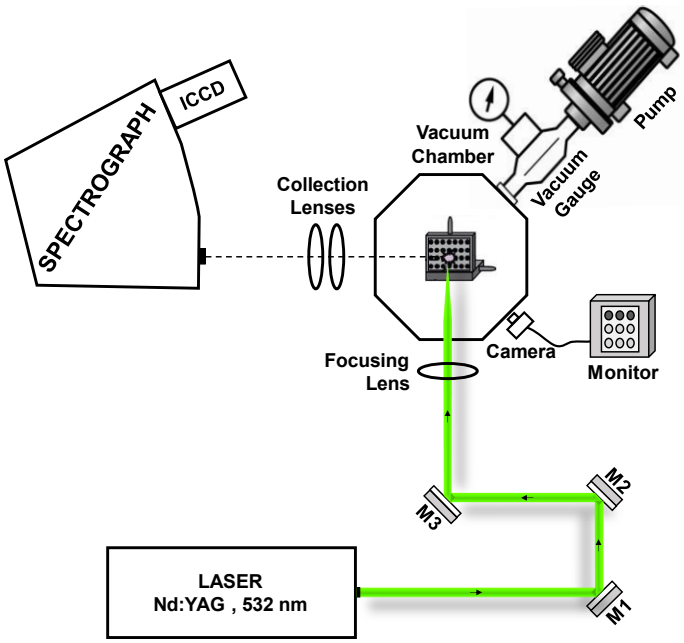

Figure 3.1. Schematic representation of experimental LIBS set-up.

3.2 Silicon Wafers

Si-wafer substrates used during the experiments were a p-type crystalline silicon wafer (c-Si), a thermally oxidized silicon wafer with 300 nm oxide coating layer (SiO_2+Si), and 75 nm, 300 nm, 450 nm, and 1000 nm nitride-coated silicon wafer substrates (Si_3N_4+Si) were obtained from MicroChemicals GmbH. In order to determine the loading area of the sample droplets, the wafers were marked in a circle shape with a fiber laser at the Izmir Laseral company.

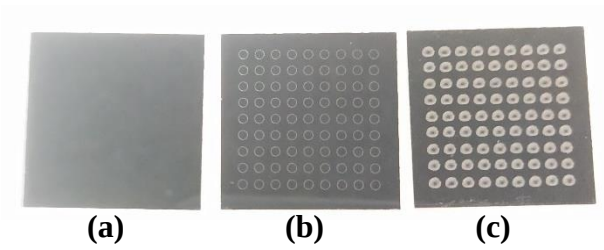

Figure 3.2. Piece of p-type c-Si wafer (25x25mm) (a) before marking (b) after marking (c) after laser shot.

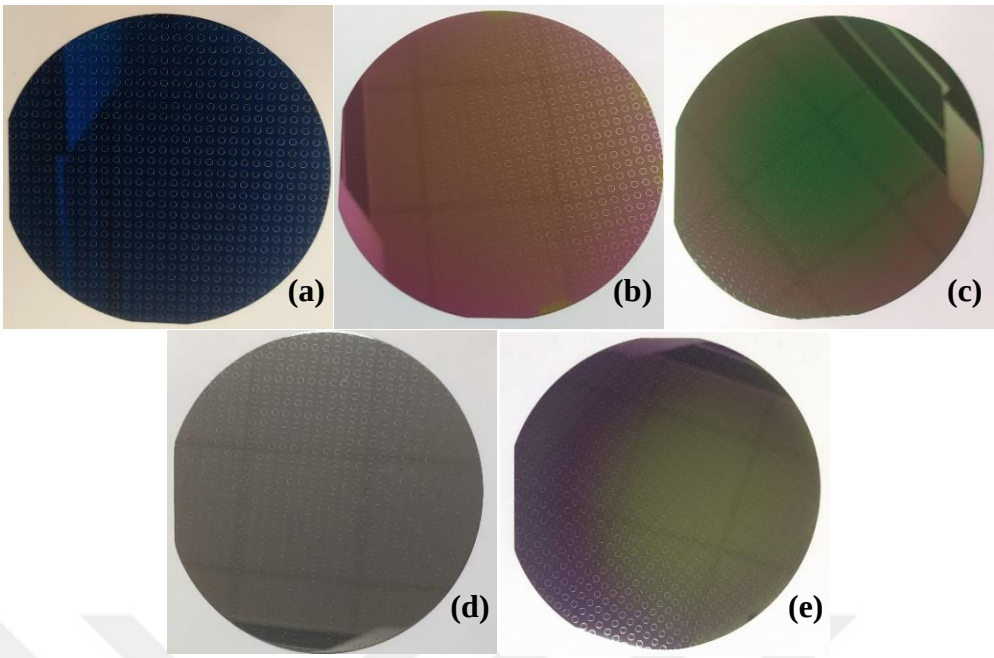

Figure 3.3. a) 75 nm b) 300 nm c) 450 nm d) 1000 nm Si_3N_4 coated (e) 300 nm SiO_2 coated silicon wafers.

3.3 Chemicals

The aqueous standard solution of cadmium was prepared from the stock solution (1000 mg L^{-1}, High Purity Standards) in 2% HNO_3 by appropriate dilution with ultrapure water. Standard cadmium solutions adjusted experimental optimization parameters and created calibration graphs. Method validation studies were performed using High Purity Solution DWPS-A-100.

The stock solutions of bovine serum albumin (4.0×10^2 μg mL^{-1}) were prepared by dissolving the solid BSA in 1X PBS buffer at pH 7.4 and stored at 0–4 °C. Sodium chloride (Sigma-Aldrich), disodium phosphate (Merck), potassium dihydrogen phosphate (Sigma-Aldrich), potassium chloride (Sigma-Aldrich), and high-purity hydrogen chloride (Merck) were used to prepare buffer solution for incubation under physiological conditions.

3.4 Methodology

3.4.1 Cadmium Binding to BSA

To mimic intracellular saline and pH conditions, bovine serum albumin (Sigma-Aldrich A3782) was incubated with cadmium (240 µM) at a molar ratio of 1:40 in a PBS buffer (pH 7.4) solution containing NaCl (137 mM). Then, the solutions were incubated at 37 °C in a heat block (VWR Standard Heat Block 13259-030). Control samples were prepared by incubating the proteins under the same conditions without cadmium solution. To remove unreacted cadmium and small molecular weight components, sample solutions were filtrated with 50 kDa cut-off filters (Amicon Ultra-0.5 mL Ultracel-50, Millipore) by centrifugation at 14,000 × g for 12 minutes. Then, 0.1 M HCl was added to the filter, and the filter was reversed. The fraction containing cadmium-bound proteins was collected by centrifugation at 1000 × g for 3 minutes.

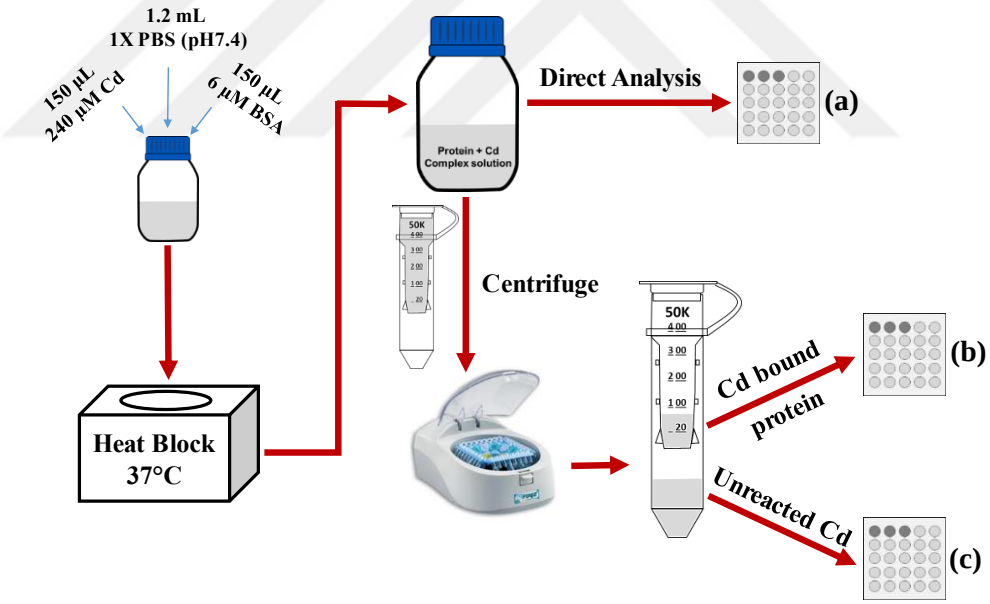

Figure 3.4. Steps of BSA bound Cd analysis by dry droplet methodology. (a) Protein-Cd complex solution (b) Cd bound protein (c) unreacted Cd analysis.

3.4.2 Whey Protein Isolation from Milk

Milk is a complex colloid containing many substances like fat, water, casein, whey, lactose, and minerals. First, the milk was heated to a boiling point to remove the fat in regular cow milk, and the floating fat was removed. Calcium caseinate is insoluble in solutions with a pH lower than 4.6. So, 1M HCl precipitated casein by lowering the pH. While the acid was slowly added to the milk and constantly stirred. The gravity filtration method was applied to remove the precipitated casein from the solution. The clear solution obtained after filtering is called whey protein solution. Absorbance measurements of whey protein were made with a spectrophotometer Shimadzu UV-2550.

Figure 3.5. Steps of whey protein isolation from milk.

3.4.3 Cadmium Binding to Whey Proteins

Isolated whey protein solution was incubated with standard cadmium solution at 37 ºC in a heat block (VWR Standard Heat Block 13259-030). To remove unreacted cadmium and small molecular weight components of the mixture, sample solutions were filtrated with 3 kDa cut-off filters (Amicon Ultra-0.5 mL Ultracel-3, Millipore) by centrifugation at 14,000 × g for 32 minutes. Then, after adding 0.1 M HCl to the filter, the filter was reversed, and the fraction containing cadmium-bound proteins was also collected by centrifugation at 1000 × g for 3 minutes.

To analyze whey proteins, samples taken directly from the solution after incubation of protein and cadmium at 37 ºC were called complex solution and analyzed with the dried droplet technique. Sample solutions were then centrifugally filtered with cut-off filters to remove unreacted cadmium. Unreacted cadmium was collected and loaded onto c-Si wafers and then analyzed. For Cd-bound fraction analysis, 0.1 M HCl was added to the filter, and the filter was inverted, Cd-bound proteins were collected by

reverse spin centrifugation. After analysis of each fraction, the results were compared and evaluated.

3.5 Dried Droplet Analysis

Within the scope of this thesis, liquid samples in a volume of 500 nL were loaded directly onto silicon wafers without applying any extra sample preparation method. Dry droplet methodology includes 3 main steps: loading, drying, and analysis. First, 500 nL of sample solution is loaded onto the silicon wafer. The drops are then dried for approximately 5 minutes and analyzed.

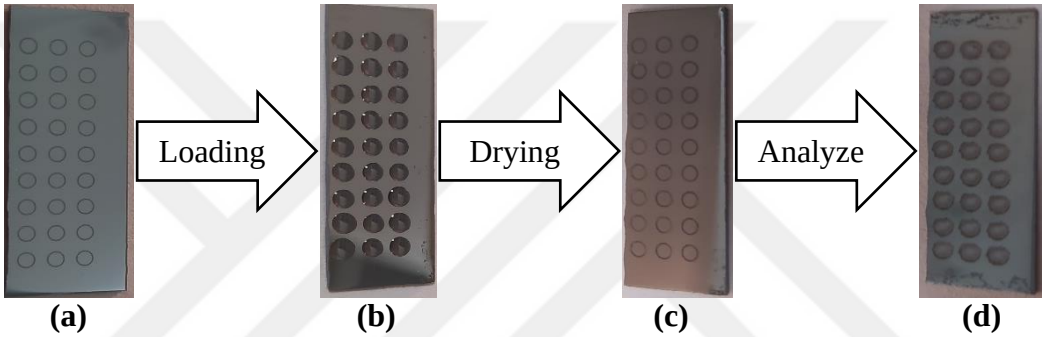

Figure 3.6. Steps of dried droplet analysis. (a) marked c-Si wafer (b) c-Si wafer after loading 500 nL sample as droplets into the marked regions (c) c-Si wafer after drying the loaded droplets (d) craters formed after laser analysis of dried droplets.

CHAPTER 4

RESULT AND DISCUSSION

This part of the thesis study presents the experimental results from the optimization and application studies for laser-induced breakdown spectroscopic detection of Cd. The optimization studies, with an emphasis on Cd signal enhancement, investigated the effect of the substrate type, ambient pressure, and experimental LIBS parameters (detector timing parameters and laser pulse energy). The quantitative determination of free Cd and protein-bound Cd in whey samples was carried out within the scope of the application studies of the developed method to real samples.

4.1 Optimization of the Experimental Conditions for Cd Detection

In the experiments carried out to determine the optimum conditions to be used in cadmium detection by LIBS, the variation of the signal intensity with substrate type, ambient pressure, detector timing parameters (delay time and gate width) and laser pulse energy were studied. The observable emission lines of the cadmium element between the 200-800 nm spectral range are given in the representative LIBS spectra in Figure 4.1., below. In addition, the neutral (I) and ionic (II) Cd emission lines observed in the LIBS spectra are listed in Table 4.1., with relevant spectroscopic information.

Radiative transitions from higher energy levels to the ground state observed at 214.44 nm, 226.50 nm, and 228.80 nm are all in the UV region. Therefore, a spectrograph with a grating of enhanced UV sensitivity was useful in qualitative and quantitative analyses of Cd. This spectrograph equipped with a Czerny-Turner-type spectrometer coupled to an ICCD detector provided more comprehensive spectral information in small wavelength intervals for each sampling.

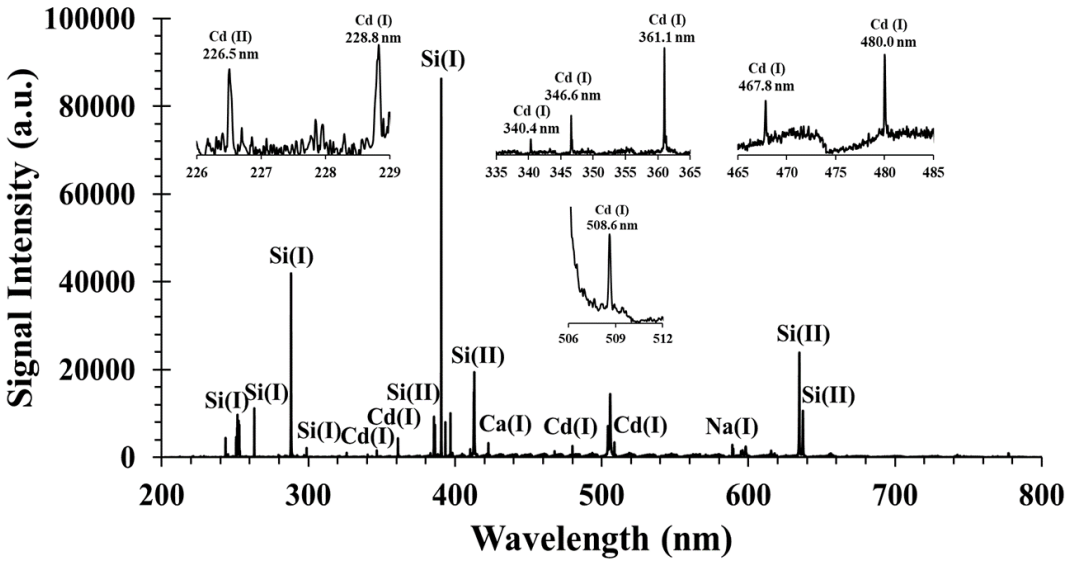

Figure 4.1. Representative LIBS spectra were obtained from 500 nL dried droplets of 1 ppm Cd with a laser pulse energy of 140 mJ, delay time of 500 ns, and gate width of 500 µs. Spectra was recorded with an echelle-type spectrometer.

Table 4.1 Emission wavelengths of cadmium to zero energy level, ionization energies, lower and upper-level configurations.

	Observed Wavelength	E_i (cm^{-1})		E_k (cm^{-1})	Lower Level Configuration		Upper Level Configuration
Cd II	214.44	0.000	-	46 618.55	$4d^{10}5s$	-	$4d^{10}5p$
Cd II	226.50	0.000	-	44 136.08	$4d^{10}5s$	-	$4d^{10}5p$
Cd I	228.80	0.000	-	43 692.384	$4d^{10}5s^2$	-	$4d^{10}5s5p$

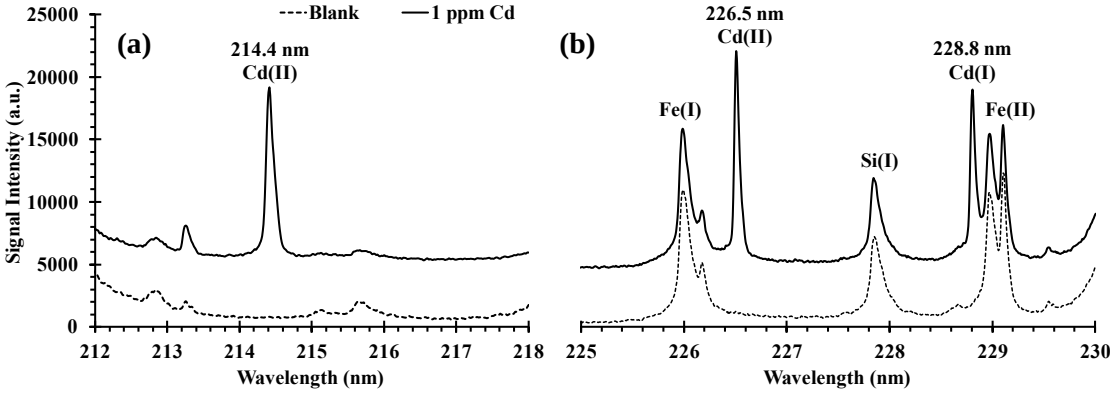

Figure 4.2. LIBS spectra from 1 mg L^{-1} Cd solution, with Czerny-Turner spectrometer equipped with 3600 g/mm grating. Wavelength range of a) 212 nm to 218 nm, and b) 225 nm to 230 nm was used. Laser pulse energy of 140 mJ, T_d =500 ns, T_g= 500 µs, 2 shot accumulation.

LIBS spectra recorded from the Cd solution at two different wavelength ranges, (212 nm - 218 nm) and (225 nm - 230 nm), are given in Figure 4.2(a-b), respectively. Each spectrum is obtained from accumulating plasma emission signals with two sequential laser pulses on the sample. The sample is 500 nL droplets of 1 ppm Cd solution and is used after drying on the silicon-wafer substrate. Since the size of the manually loaded droplets on the Si-wafer substrate, before drying, was 1.3 mm in diameter, and in order for a laser beam to cover all sampling area, the laser beam size was adjusted by changing the lens-to-sample distance. Among several Cd lines observed, the ionic line, Cd (II) at 226.5 nm, was the most intense, therefore, most of the evaluation studies are performed on the data of this wavelength.

4.1.1 The Effect of Substrate Type on Cd Signal Intensity

Most literature studies are based on using liquid-to-solid conversion strategies for liquids analyses by LIBS utilizing metal substrate to observe the analyte enhancement effect. These substrates can be aluminum, zinc, and copper. There are few studies on using non-metallic substrates in LIBS analyses via dried droplet methodology. We have been using non-metallic Si-wafer substrates in our laboratory for quite a time, and the analytical performance of the various substrates for heavy metals (Cu, Cr, Mn, Cd, and Pb) detection was determined. In this thesis study, several substrate surfaces, crystalline silicon (c-Si), 300 nm oxide-coated silicon (SiO_2+Si), and 75nm, 300 nm, 450 nm, and 1000 nm silicon nitride-coated silicon (Si_3N_4+Si), were tested for their ability for signal enhancement in Cd detection. Figure 4.3 shows the comparative results in terms of both signal intensity (left y-axis) and signal-to-noise ratio (right y-axis) variation of Cd (II) 226.5 nm line with respect to Si-wafer substrates of different coatings and different coating thicknesses.

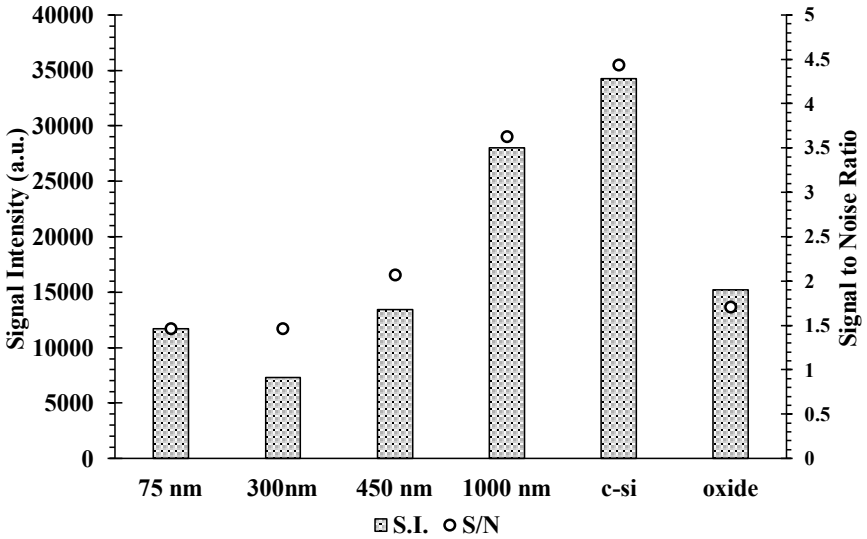

Figure 4.3. Comparison of the signal intensity (left) and signal-to-noise ratio (right) variation with Si-wafer substrates of different coatings and different coating thicknesses.

When the Cd signal from different coating thicknesses of silicon nitride substrate is considered, as can be seen in Figure 4.3., the Cd signal increases as the coating thickness increases, except the 75 nm silicon nitride-coated Si-wafer substrate shows a stronger Cd signal than the one with 300 nm coating. This result can be explained by the thin film effect and closeness of this coating thickness to the optimum anti-reflection coating thickness of 65 nm, which can be calculated using the formula $d = \lambda/4n$. Here, d is the optimum coating thickness (nm), λ is the wavelength of the laser used (532 nm), and n is the refractive index of the coating material (2.05 for Si_3N_4). At this coating thickness, the analyte species absorb most of the laser light with minimum reflectivity on the surface. However, the signal increase observed for 450 nm and 1000 nm Si_3N_4-coated substrates are higher than the 75 nm and 300 nm Si_3N_4 coated ones. At such high coating thicknesses, the bulk physical properties of the Si_3N_4 layer, like low thermal conductivity, high heat resistance, and hardness, become effective and increase with the coating thickness.

Laser pulse energy sent to the substrate surface is used both by the analyte and the substrate material for excitation. When the Cd signals observed from the surfaces of different coating materials, crystalline silicon wafer (c-Si), Si_3N_4 coated Si- wafer (Si_3N_4+Si) and SiO_2 coated Si- wafer (SiO_2+Si) are compared, due to low band gap (1.2 eV) of c-Si compared to SiO_2 (8.9 eV) and Si_3N_4 (5.0 eV) surfaces, most of the laser

energy is transferred to the analyte for excitation. Hence, in c-Si surfaces, higher number of excited atoms goes through the emission process. Therefore, the most intense Cd signal is observed with the c-Si wafer substrate surfaces, and c-Si surfaces were selected as the most suitable substrate to be used throughout the studies in Cd detection by LIBS.

4.1.2 Effect of Ambient Pressure on Signal Intensity

The type of gas and the pressure of the ambient environment are significant factors during LIBS measurements. Several studies in literature have shown improvements in the detection power of the LIBS technique at reduced pressures. LIBS analyses at low-pressure environment conditions give better results regarding spectral intensity, signal-to-noise ratio (S/N), spectral resolution, and ablation characteristics. As the ambient pressure decreases, the number of gas molecules and, hence, the collisions and interactions between the plasma and gas molecules decrease. This results in a decrease in the noise level and enhancement in S/N.

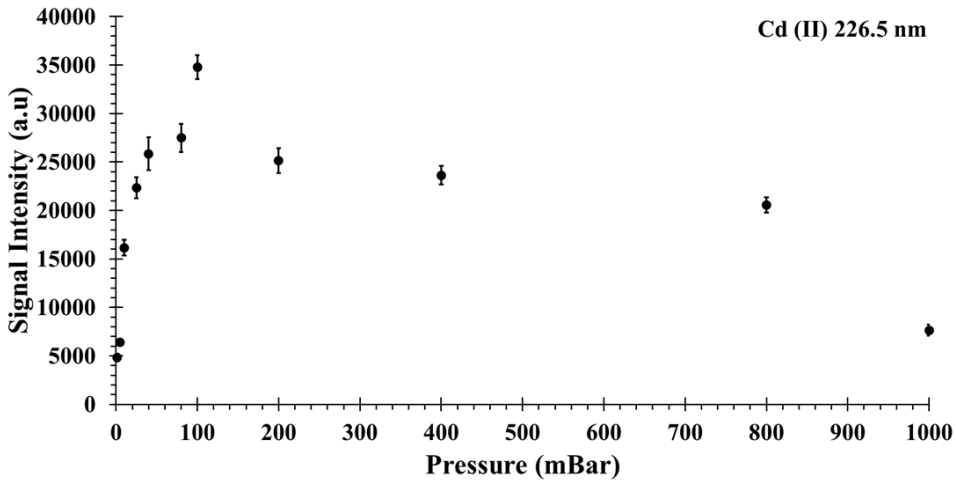

Figure 4.4. Cd signal (at 226.5nm) variation with respect to ambient pressure. Cd signal for 1 $mg.L^{-1}$ (ppm) Cd solution with Czerny-turner spectrometer of 3600 lines/mm grating.

Figure 4.4. shows the LIBS signal intensity variation of Cd (II) 226.5 nm line with respect to change in ambient pressure for 1 ppm ($mg.L^{-1}$) Cd standard solution. It is demonstrated that the signal intensity increases gradually when the ambient pressure is decreased from 1000 mbar to 100 mbar. After reaching the maximum signal intensity at 100 mbar, the signal intensity begins to decrease.

In order to further investigate this ambient pressure effect, some emission wavelengths of Cd, other than 226.5 nm were also studied. For that purpose, a multi-wavelength detector (an echelle-type spectrometer equipped with ICCD detector) was used. The results are shown in Figure 4.5. The same behavior is observed for other emission lines of Cd as in the case of the 226.5 nm emission line. The signal intensity gradually increases with increased pressure until 100 mbar, reaches its maximum level., and then, progressively reduces as the ambient pressure is increased from 100 mbar to 1000 mbar.

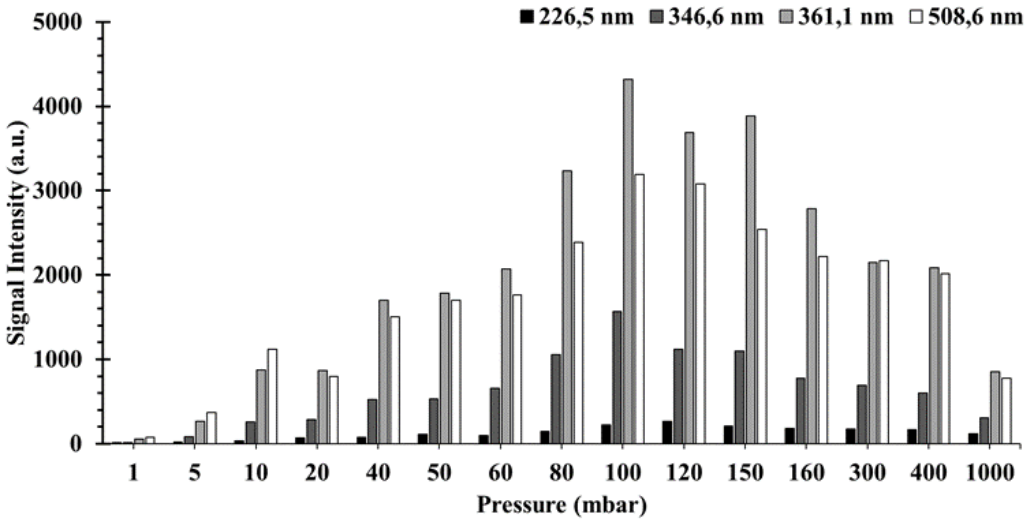

Figure 4.5. Effect of ambient pressure on different Cd emission lines for 2 ppm Cd solution dried on c-Si substrate. An echelle type spectrometer was used.

There is a significant spectral enhancement at 100 mbar pressure compared to atmospheric conditions, for all emission lines of Cd in the UV-Vis range. To better understand this pressure dependent signal enhancement mechanism, images of the plasma at various ambient pressures were taken with the help of an ICCD camera. It can be clearly observed in Fig. 4.6 that, at the 1000 mbar atmospheric pressure, the plasma is relatively small and confined to a region close to the target surface, by the surrounding atmospheric molecules. As the pressure decreases to 400 mbar, the plasma moves more freely into the ambient atmosphere, expands towards the laser, and gets bigger. This movement and enlargement cause the center of the plasma to move away from the slit of the spectrometer. Therefore, one should be careful about placing the center of the plasma on the entrance slit of the spectrograph, each time the pressure is changed. This enlargement continues until 100 mbar pressure, reaches the maximum in size and luminosity at that pressure. After that, as the pressure even decreases, the number of surrounding molecules, and the

number of collisions decreases. Since the collisions are the main sources of the most dominant excitation mechanism, plasma starts to become smaller and after 5 mbar pressure its formation is prohibited and fades away. These observations from the plasma images led us to work at 100 mbar pressures for future experiments.

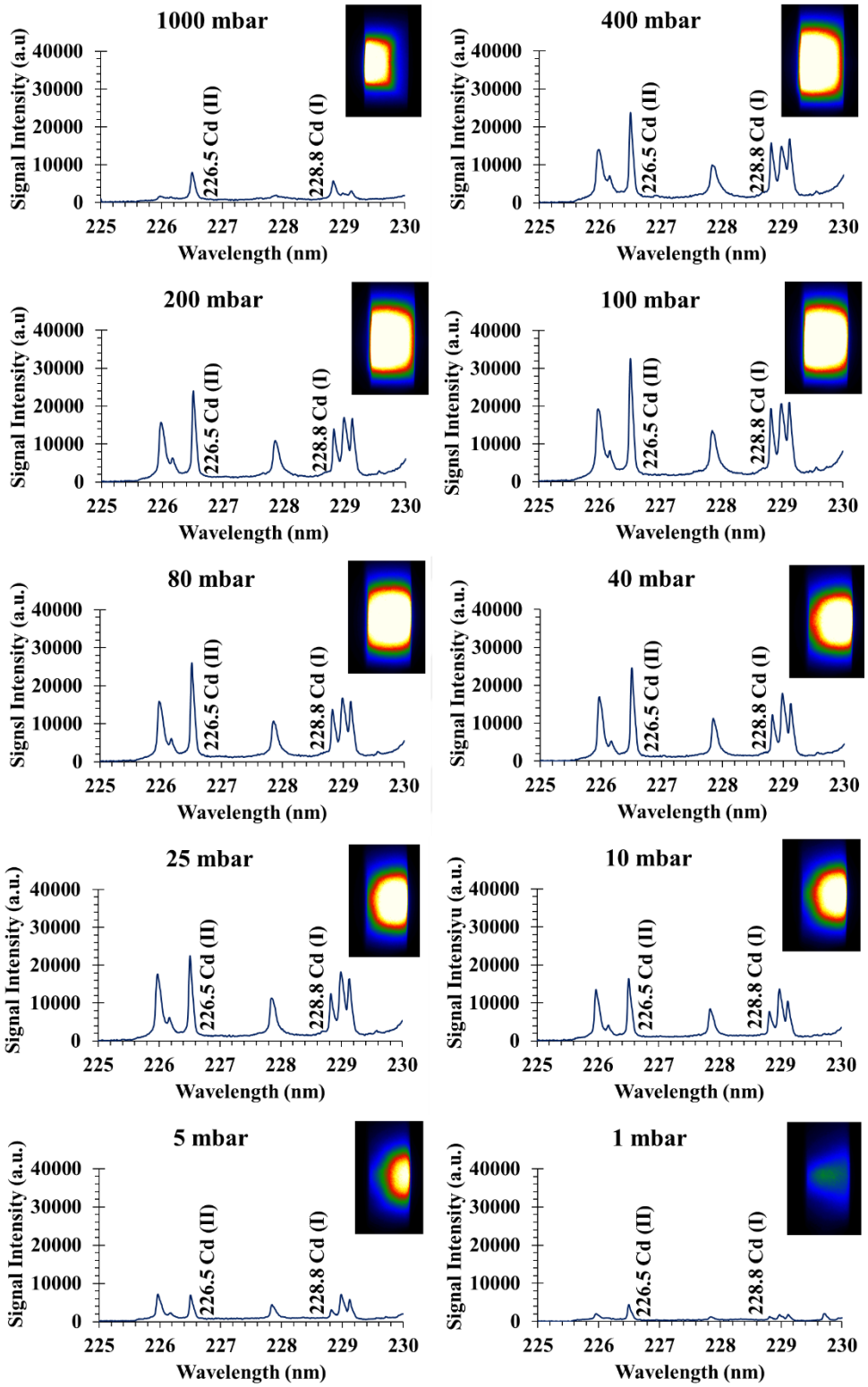

Figure 4.6. The variation in the LIBS emission signal of Cd for 1 ppm Cd solution at 226.5 nm and 228.8 nm with respect to ambient pressure and the plasma images at different ambient pressures.

4.1.3 Detector Timing Parameters

Laser-induced plasma is a time-dependent phenomenon in which several different processes occur at several stages, and it requires quantitative measurements to be performed under conditions where the signal intensity is maximum. Therefore, timing parameters such as detector delay time and gate width were examined to obtain the highest LIBS signal from the cadmium element.

4.1.3.1 Delay Time

The time between the interaction of the laser pulse and the start of data collection is the delay time. Most of the emissions consist of background radiation at the beginning of the plasma formed after the laser pulse interacts with the analyte. Then, the plasma expands and cools within a few microseconds. Therefore, experiments were performed to optimize the detector delay time (T_d) to achieve high analyte and low background signal in the LIBS spectrum.

Delay time optimization studies were carried out at atmospheric pressure and a reduced pressure of 100 mbar, which was determined as the optimum pressure. Optimization experiments were performed with constant gate width (500µs) and laser energy (140 mJ). Figure 4.7. shows the Cd(II) signal intensity change depending on the delay time. As shown, under both ambient conditions, the 226.5 nm signal intensity of the Cd(II) line increases until 500 ns delay time and then decreases. Therefore, 500 ns was chosen as the optimum detector delay time.

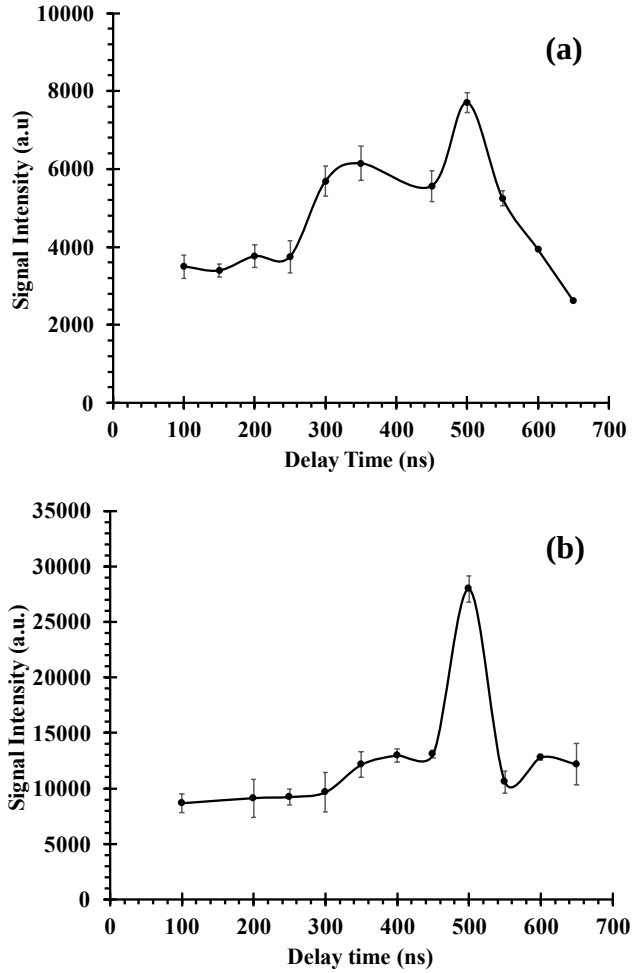

Figure 4.7. Variation of LIBS signal intensity of Cd (II) at 226.5 nm with respect to the detector delay time (a) at atmospheric pressure and (b) at 100 mbar.

4.1.3.2 Gate Width

Another important parameter for time resolution in LIBS measurements is the detector gate width (T_g), which is the duration that the detector remains open for data acquisition. Gate width optimization studies were also carried out at atmospheric pressure and optimum pressure (100 mbar), and the experiments were carried out with constant delay time (500ns) and laser energy (140 mJ). Figure 4.8. shows the signal intensity change of Cd(II) at 226.5 nm with respect to detector gate width. As seen in the figure, the same trend was observed in both environmental conditions. The 226.5 nm line intensity of the Cd(II) increased until 500 µs and then decreased. Therefore, 500 µs was chosen as the optimum detector gate width.

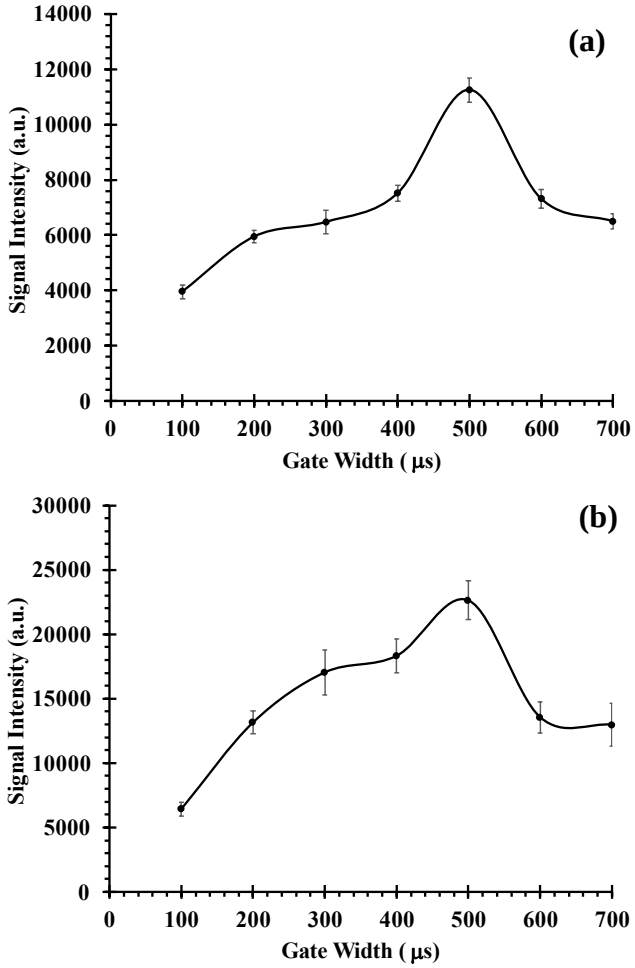

Figure 4.8. Variation of LIBS signal intensity of Cd (II) at 226.5 nm with respect to the detector gate width (a) at atmospheric pressure and (b) at 100 mbar.

4.1.4 Effect of Laser Energy

In LIBS experiments, the energy of the laser pulse plays a crucial role in the quality of laser-matter interactions and the resulting plasma formation. If the laser energy is too low, the plasma density and signal intensity will also be low, while too high laser energy can cause unpredictable ablation of the target surface and shorten the life of the laser source. A comparative analysis was performed with varying laser pulse energy to understand the effect of laser pulse energy on signal intensity, while keeping the other experimental parameters constant. Figure 4.9 shows the variation in Cd(II) signal with respect to laser pulse energy, for two ambient pressure conditions. In general, signal increases as laser pulse energy increases. Therefore, among the six different pulse

energies studied, 140 mJ pulse energy was determined as the optimum laser energy for both ambient conditions.

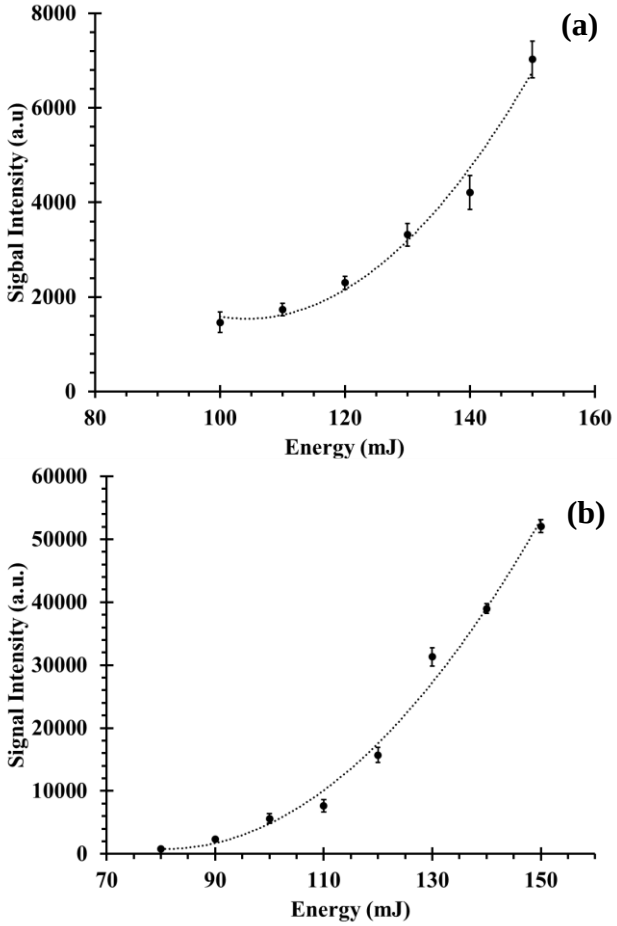

Figure 4.9. LIBS signal intensity variation of 226.5 nm Cd (II) line with respect to laser pulse energy (a) at atmospheric pressure and (b) at 100 mbar.

Table 4.2 lists the optimum experimental LIBS parameters in terms of laser pulse energy, delay time, and gate width of the detector.

Table 4.2. Optimum experimental conditions for Cadmium (Cd).

Condition	Pulse Energy (mJ)	Delay Time (T_d)	Gate Width (T_g)
Atmospheric pressure	140	500 ns	500 µs
100 mbar	140	500 ns	500 µs

4.2 Quantitative Analysis of Cd in Aqueous Environments

4.2.1 Calibration Studies

The ability of dried-droplet LIBS methodology for quantitative analysis of Cd at reduced pressures was investigated using single standard solutions and certified reference water samples. For this, calibration curves were created, and performance characteristics such as limit of detection, accuracy, precision were evaluated.

Calibration curves for Cd were generated under two different ambient conditions by utilizing known concentration single element standards. The signals were obtained by accumulating the laser pulses of 140 mJ energy for 5 separate dried-droplets, and the average signal value was used in the graphs. Relative signal intensity values were derived from peak heights of atomic emission lines, with the background emission subtracted. To calculate error bars, standard deviations of the replicate measurements were employed. The calibration graphs constructed from their respective LIBS measurements are shown in Figure 4.10. The LOD was determined for each ambient pressure condition.

According to the IUPAC definition, the limit of detection (LOD) is calculated as LOD = 3 σ_{BG} / m, where σ_{BG} represents the standard deviation of the background and m represents the slope of the calibration curve. LOD values calculated from calibration curves are given in Table 4.3., in absolute amount and in concentration units. Literature values are changing from one to another and each has a different approach. When this study was compared to other cadmium studies in the literature, especially for reduced pressure system, improvement was observed in the detection limit for cadmium element.

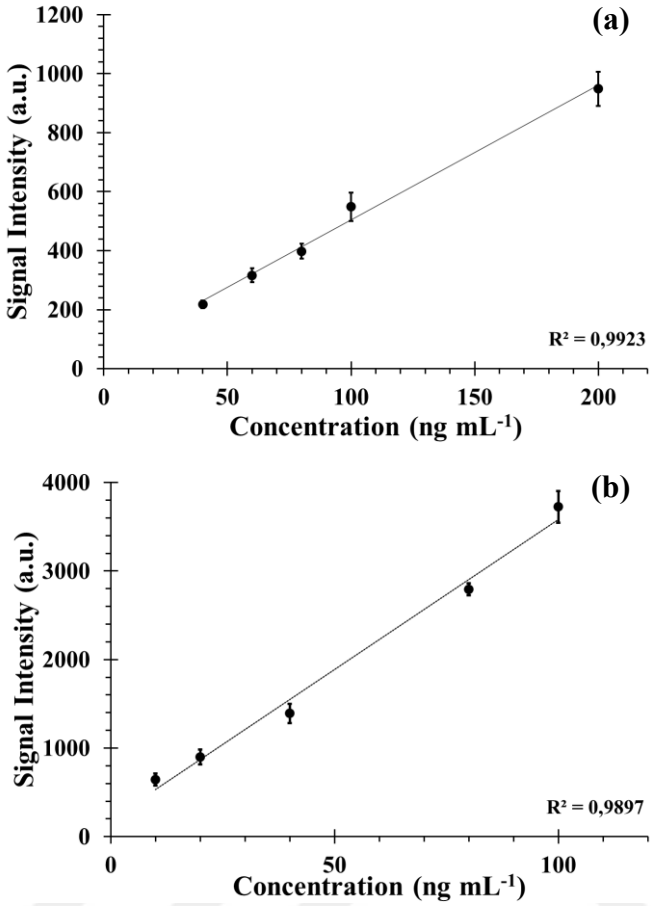

Figure 4.10. Calibration curves for Cd (II) 226.5 nm (a) at atmospheric pressure and (b) at 100 mbar reduced pressure conditions.

Table 4.3. Some concentration based LOD values from the literature for Cd.

	Limits of Detection (LOD)		Sample Methodology	
	pg	ng mL^{-1}		
Atmospheric pressure		11	Agarose film-based liquid-to-solid conversion	You et al., 2023
Atmospheric pressure		4.86	Electrodeposition on a polished Al	Ma et al., 2022
Atmospheric pressure		220	Dried droplet on SSH Substrate	Zhu et al., 2022
Atmospheric pressure		8.9	Liquid to solid conversion on Zn	Ma et al., 2020
Atmospheric pressure		4.6	Metal-chelate induced nanoparticle aggregation	Liu et al., 2020
Atmospheric pressure		165	Filter paper enrichment	Xiu et al., 2020
Atmospheric pressure		3.6	Chelating resin enrichment	Tian et al., 2019
Atmospheric pressure		24	Dispersive micro solid-phase extraction with graphene oxide	Ruiz et al., 2019
Atmospheric pressure	6.8	13.6	Dried-droplet on a crystalline silicon wafer (c-Si)	This work
100 mbar	1.1	2.1		This work

4.2.2 Method Validation Experiments

To validate the methodology at reduced pressures, the certified multi-element standard DWS (Drinking Water Standard) was used. The standard was diluted to a final analyte concentration of 50, 500 and 5000 ng mL^{-1} and analyzed under optimum conditions. The ratio of the difference between the found value and the reference value to the reference value was used to calculate the percentage error values using the given equation (3.1).

$$\% \, Error = \frac{Measured \;\; Value \; - Reference \;\; Value}{Reference \;\; Value} x \, 100 \qquad (3.1)$$

The relative standard deviation of three measurements was used to derive the precision values and the percentage precision values were calculated by using the given equation (3.2). Experiments were carried out at 100 mbar ambient pressure, and the results are listed in Table 4.4.

$$\% \, Precision = \frac{Standard \quad deviation \quad of \ replicate \quad measurements}{Mean} \, x \, 100 \qquad (3.2)$$

Table 4.4. Performance characteristics of dried-droplet LIBS at reduced pressures.

	Certified Material (µg mL^{-1})	**Dilution Factor**	**Diluted Solution (ng mL^{-1})**	**Measured Concentration (ng mL^{-1})**	**Error (%)**	**Precision (%)**
Cd (II)*	50.0	10	5000.0	5349.6	+7	10
Cd (II)*	50.0	100	500.0	569.4	+14	10
Cd (II)*	50.0	1000	50.0	43.6	-13	11

(*) - DWS-Drinking Water Metal Solution - DWPS-A-100.

4.3 Application of the Methodology to Real Sample Analysis

An application of Cd detection by LIBS in reduced-pressure environments was performed on Cd-binding proteins. In living systems, most cadmium binds to plasma proteins and exhibits various interactions with proteins through covalent binding with amino acids, especially cysteine. As a real sample, whey protein obtained from milk consists of ß-lactoglobulin, α-lactalbumin, serum albumin, immunoglobulins, and lactoferrin fractions. Serum albumin can bind to heavy metals such as cadmium and help transport them due to the cysteine residues it contains. For this purpose, standard protein Bovine Serum Albumin (BSA) and whey protein samples extracted from the milk were incubated in standard Cd solution for several hours at 37 °C. The sample solutions underwent filtration through cut-off filters via centrifugation. The unreacted cadmium in a liquid filtrate and the fraction containing cadmium-bound protein was collected and analyzed individually on c-Si substrates via dried-droplet methodology.

4.3.1 Incubation Studies of Cd and Bovine Serum Albumin (BSA) Standard

LIBS experiments were initially performed to understand the interactions between cadmium and the molar concentration ratio of bovine serum albumin, BSA protein, over the time. For that purpose, Cd solutions of definite concentration were incubated with BSA protein at different incubation times (16, 24, and 48 hr). When the incubation period was over, the complex solution was filtered with centrifugal cut-off filters. After the filtration process, free cadmium ions (not bound to the proteins) were collected in the filtrate part, whereas Cd-bound proteins were collected on the filter and then taken back to the solution for Cd determination after a few times washing processes.

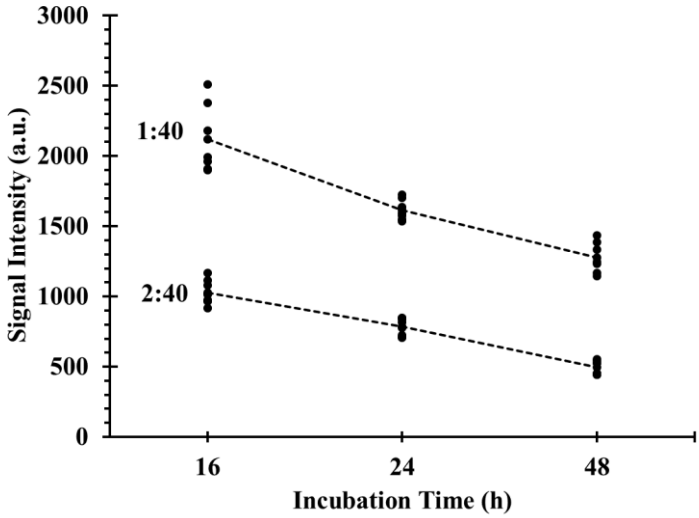

Figure 4.11. Change in the unbound free Cd (II) signal intensity at 226.5 nm obtained as a result of bovine serum albumin and cadmium incubation at different incubation times (16, 24, and 48 hours) and molar concentration ratios (1:40 and 2:40 BSA: Cd).

The variation of the LIBS signal intensity obtained from the filtrate (unbound Cd) according to different incubation times and its molar ratios are shown in Figure 4.11. As the incubation time increased, the amount of unbound cadmium in the solution decreased. Also, when the amount of cadmium in the solution was kept constant, and the amount of protein increased, more cadmium was bound to the protein.

Results from the LIBS experiments showing the effect of incubation time between bovine serum albumin and Cd on free and bound Cd are shown in Figure 4.12. In this

experiment, the BSA:Cd ratio was 1:40 molar, and the values in the graph were obtained from the Cd (II) signal intensity at 226.5 nm. As a result of incubation studies at a constant temperature, the complex solution taken from the solution for each hour to be studied was filtered with centrifugal cut-off filters. The Cd ions bound to the protein, and those not bound in the solution were separated. Both fractions were loaded onto the substrate using the dried droplet method and analyzed with LIBS. The decreasing Cd signal in the filtrate as the incubation time increased is an indication of the increased amount of Cd-bound protein, and after the 24th hour, this increase was less than the one in the first hours. For this reason, an incubation period of 26 hours was used in the experiments throughout this thesis study.

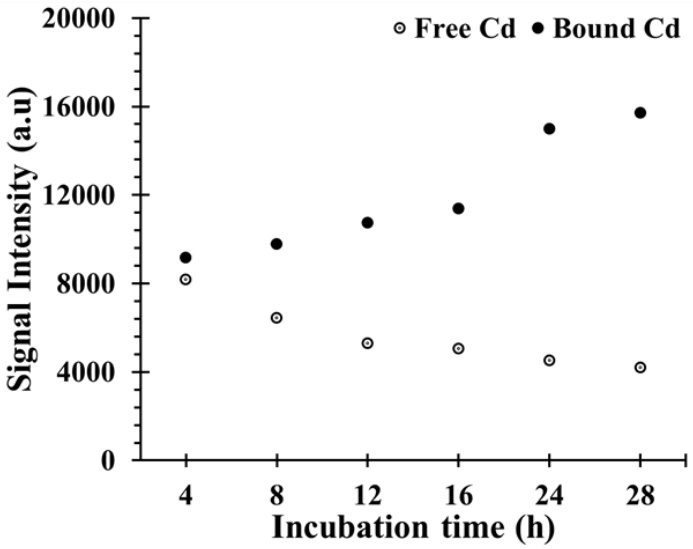

Figure 4.12. LIBS signal intensity variation with respect to incubation time for bound and unbound free-Cd to BSA with a 1:40 molar ratio of BSA: Cd.

To determine the accuracy of the method used, after the incubation at 37 °C and 26 hours, the unfiltered complex solution (containing free Cd and protein-bound Cd), the filtrate (containing free Cd), and the complex (protein-bound Cd) taken by washing after filtration were analyzed separately. As is shown in Figure 4.13., the summation of the LIBS signal intensities of unreacted free Cd and the protein-bound Cd agrees with the signal observed from the unfiltered BSA-Cd complex solution.

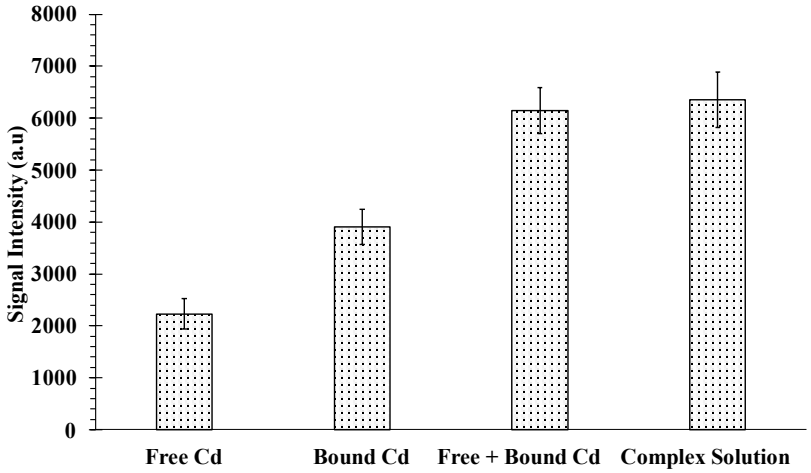

Figure 4.13. LIBS signal intensities of unreacted (free) Cd and the fraction containing Cd-bound protein equal the signal observed from unfiltered BSA-Cd complex solution after 26 hours of incubation at 37 °C.

4.3.2 Incubation Studies of Cd and Whey Protein Extracted From Milk

Cow's milk protein consists of two prominent protein families. About 80% of the total protein represents insoluble caseins; the remaining 20% represents soluble whey proteins. Whey protein is a high-quality protein derived from milk, and it contains various proteins; the primary ones are α-lactalbumin, β-lactoglobulin, lactoferrin, and serum albumin. The presence of whey protein, obtained by removing fat and casein from milk, is detected by UV-Vis spectrophotometry with an absorption peak at 280 nm, indicating the protein's presence. The absorbance spectra between 200-340 nm and a calibration graph constructed for whey concentration (%)versus corresponding absorbance values at their peak maxima are shown in Figure 4.14.

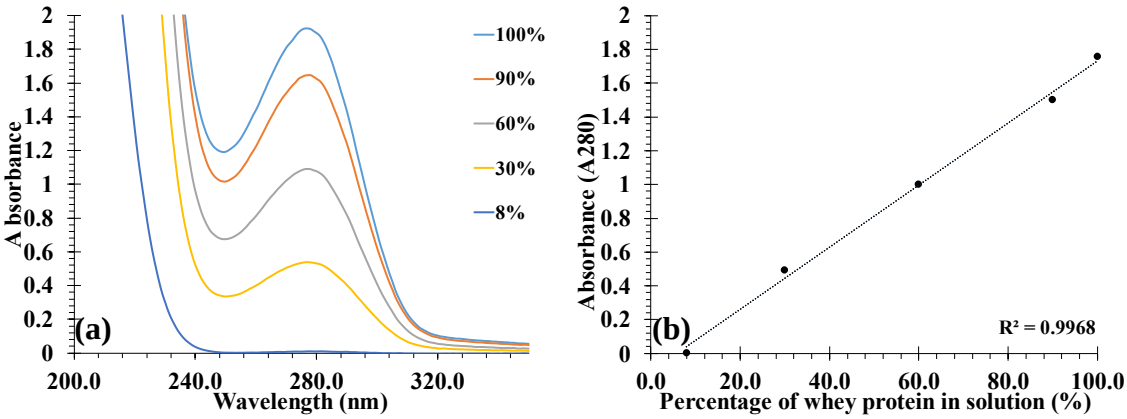

Figure 4.14. (a) UV-Vis spectra of whey protein extracted from milk by percentage in solution. (b) The relationship between the percentage of whey protein in a solution and the corresponding absorbance value.

After a 16-hour incubation period at 37°C, separate analyses on the unfiltered complex solution containing free Cd and Cd-bound protein and the free and protein-bound Cd obtained after filtration of the complex solution were carried out. Figure 4.15., illustrates that the summation of the LIBS signal intensities of unreacted free Cd and the protein-bound Cd is equivalent to the observed signal from the whey-Cd complex solution.

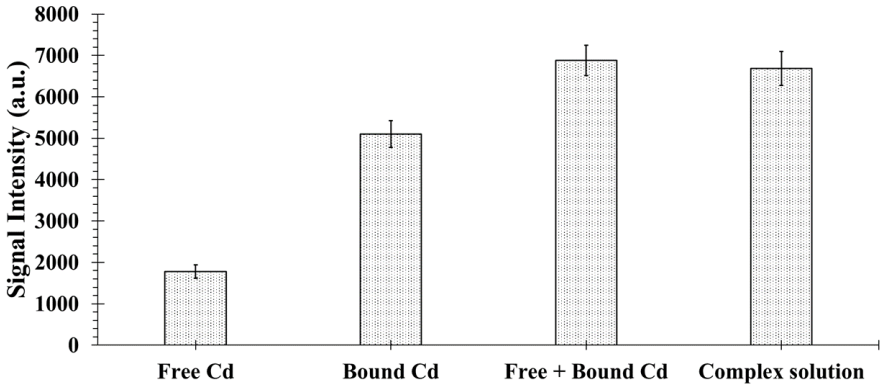

Figure 4.15. LIBS signal intensities of unreacted (free) Cd and the fraction containing Cd-bound protein equal the signal observed from unfiltered whey-Cd complex solution.

In order to examine how the dilution factor of whey affects the cadmium signal, the experiments were carried out under the same conditions. While the amount of

cadmium in the total solution was kept constant, the amount of whey was changed as percentages. The relationship between Cd-signal (226.5 nm) and whey concentration (%) on the Cd(II) signal intensity is shown in Figure 4.16. The 0.0% value in the graph represents the cadmium signal obtained when there is no whey protein in the medium.

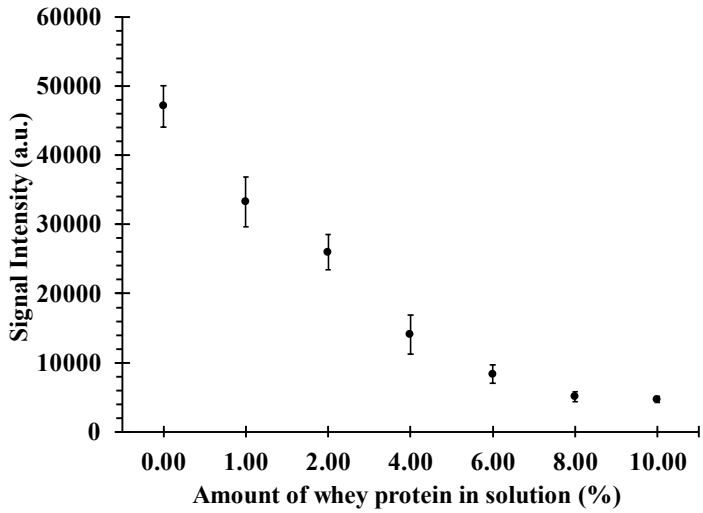

Figure 4.16. Variation of 226.5 nm Cd(II) signal intensity with varying amounts of whey protein in the total solution.

To measure the quantitative analysis ability of the method, the whey protein solution was diluted to 1% to reduce the matrix effect, and standard cadmium solutions at different concentrations were incubated. The calibration curve was created, and the detection limit for the whey protein matrix solution was evaluated. The signals were obtained for 5 separate droplets, and the average signal value was used in the graphs. Relative signal intensity values were derived from peak heights of atomic emission lines, with the background emission subtracted. To calculate error bars, standard deviations of the replicate measurements were employed. The calibration graph constructed from respective LIBS measurements and the calculated limit of detection value is shown in Figure 4.17. The LOD value was calculated as 20.2 ng mL^{-1} (ppb), which means that the absolute detection amount of Cd bound to whey proteins was 10 picograms.

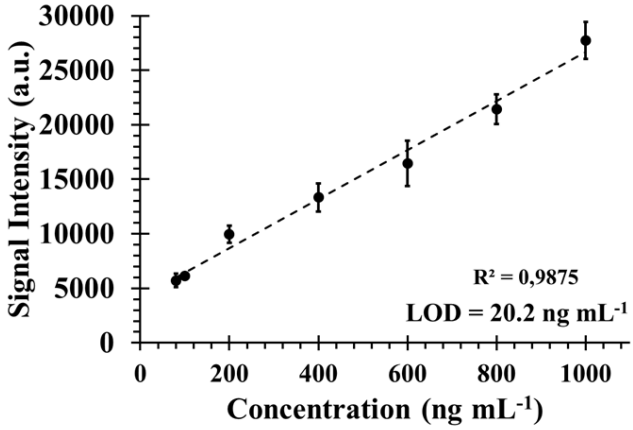

Figure 4.17. Calibration curve for whey protein-Cd complex solution. The extracted whey protein was diluted to 1% in the final solution.

Preconcentration studies have been carried out to detect lower cadmium concentrations in the whey protein matrix. A complex solution has been prepared so that 1% of the total solution by volume is whey protein. Figure 4.18. shows the signal intensities obtained in preconcentration studies. The results show that the method is reproducible, and lower cadmium concentrations can be detected with the preconcentration method.

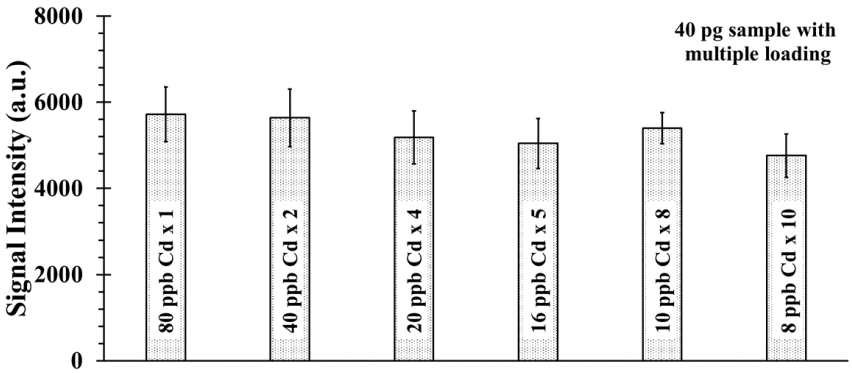

Figure 4.18. LIBS signal intensities of whey protein-Cd complex solution preconcentration studies. The whey protein used was diluted as 1% in the final solution.

CHAPTER 5

CONCLUSIONS

In this thesis study, low-pressure LIBS measurements were performed to improve the detection power of the dried-droplet LIBS methodology for the determination of Cd in aqueous and in biological matrices. 100 mbar pressure was found as the optimum for most emission lines of Cd. Results showed improvements in signal intensity and hence, in detection limits. Detection limits of Cd in absolute amounts of 6.8 picograms and 1.05 picograms were obtained at atmospheric pressure and 100 mbar pressures, respectively. Results showed that 6.5 times effective signal enhancement occurs for Cd measured at 100 mbar pressures compared to measurements at 1-atm. conditions. Among several Si-wafer based substrates, the c-Si substrate was found to show the highest signal enhancement for Cd detection.

Incubation studies of cadmium with BSA and whey proteins were performed. The summation of the LIBS signal intensities of unreacted (free) Cd and the Cd-bound protein was found equal to the signal observed from the BSA-Cd complex solution after incubation at 37 ºC. This indicates the capability of the dried-droplet LIBS methodology for the quantitative determination of Cd bound to proteins in biological environments. The detection of 10 picograms of Cd bound to whey proteins was demonstrated.

LIBS is a fast and sensitive optical spectroscopic technique that does not require sample preparation steps. This study demonstrates that LIBS is a suitable method for identifying Cd bound to whey proteins in an aqueous medium with a detection capacity in the order of picograms.

REFERENCES

Ahamer, C. M., Pedarnig, J. D. 2018. Femtosecond double-pulse laser-induced breakdown spectroscopy: Investigation of the intensity enhancement. Spectrochimica Acta Part B: Atomic Spectroscopy, 148, 23–30.

Alhasmi, A. M., Gondal, M. A., Nasr, M. M., Shafik, S., Habibullah, Y. B. 2015. Detection of toxic elements using laser-induced breakdown spectroscopy in smokers' and nonsmokers' teeth and investigation of periodontal parameters. Applied Optics, 54(24), 7342.

Arabi, D., Hamdy, O., Mohamed, M., S., M., Salam, Z., A., Harith, M., A. 2023. Discriminating two bacteria via laser-induced breakdown spectroscopy and artificial neural network. AMB Express, 13, 61.

Aras, N., Ünal, S., Arıca, D., Yalçın, Ş., 2012. Ultrasonic nebulization-sample introduction system for quantitative analysis of liquid samples by laser-induced breakdown spectroscopy. Spectrochimica Acta Part B: Atomic Spectroscopy. 74-75, 87-94.

Aras, N., Yalçın, Ş. 2014. Rapid identification of phosphorus containing proteins in electrophoresis gel spots by Laser-Induced Breakdown Spectroscopy, LIBS. Journal of Analytical Atomic Spectrometry, 29(3), 545–552.

Aras, N., Yalçın, Ş. 2016. Development and validation of a laser-induced breakdown spectroscopic method for ultra-trace determination of Cu, Mn, Cd and Pb metals in aqueous droplets after drying. Talanta, 149, 53–61.

Aras, N., Yalçın, Ş. 2019. Investigating silicon wafer based substrates for dried-droplet analysis by Laser-Induced Breakdown Spectroscopy. Spectrochimica Acta Part B: Atomic Spectroscopy, 152, 84–92.

Bae, D., Nam, S.-H., Han, S.-H., Yoo, J., Lee, Y. 2015. Spreading a water droplet on the laser-patterned silicon wafer substrate for surface-enhanced laser-induced breakdown spectroscopy. Spectrochimica Acta Part B: Atomic Spectroscopy, 113, 70–78.

Bashir, S., Dawood, A., Hayat, A., Askar, S., Ahmad, Z., Ahmad, H., Khan, M., A. 2023. Laser-assisted plasma formation and ablation of Cu in a controlled environment. Heliyon, 9, 8, e18781.

Berlo, K., Xia, W., Zwillich, F., Gibbons, E., Gaudiuso, R., Ewusi-Annan, E., Chiklis, G., R., Melikechi N. 2022. Laser induced breakdown spectroscopy for the rapid detection of SARS-CoV-2 immune response in plasma. Scientific Reports 12, 1614.

Botto, A., Campanella, B., Legnaioli, S., Lezzerini, M., Lorenzetti, G., Pagnotta, S., Poggialini F., Palleschi, V. 2019. Applications of Laser-Induced Breakdown Spectroscopy to Cultural Heritage and Archaeology: a critical review. Journal of Analytical Atomic Spectrometry, 34, 81–103.

Brouard, D., Gravel, J.-F. Y., Viger, M. L., Boudreau, D. 2007. Use of sol–gels as solid matrixes for laser-induced breakdown spectroscopy. Spectrochimica Acta Part B: Atomic Spectroscopy, 62(12), 1361–1369.

Burger, M., Finney, L. A., Garrett, L., Harilal, S. S., Hartig, K. C., Nees, J., Skrodzki, P., J., Xiao, X., Jovanovic, I. 2021. Laser ablation spectrometry for studies of uranium plasmas, reactor monitoring, and spent fuel safety. Spectrochimica Acta Part B: Atomic Spectroscopy, 179, 106095.

Chaudhary, K., Rizvi, S. Z. H., Ali, J. 2016. Laser-induced plasma and its applications. Plasma Science and Technology - Progress in Physical States and Chemical Reactions.

Chen, X., Li, X., Yang, S., Yu, X., Liu, A. 2018. Discrimination of lymphoma using laser-induced breakdown spectroscopy conducted on whole blood samples. Biomedical Optics Express, 9(3), 1057.

Chen, Z., Godwal, Y., Tsui, Y. Y., Fedosejevs, R. 2010. Sensitive detection of metals in water using laser-induced breakdown spectroscopy on wood sample substrates. Applied Optics, 49(13), C87.

Cheng, D., Zhao, T., Zhou, J., Yao, C., Xi, Y. 2022. Comparative investigation on the influence of chlorogenic acid and its intestinal metabolites on the binding of cadmium to bovine serum albumin, Journal of Molecular Liquids, 366.

Choi, J.-J., Choi, S.-J., Yoh, J. J. 2016. Standoff detection of geological samples of metal, rock, and soil at low pressures using laser-induced breakdown spectroscopy. Applied Spectroscopy, 70(9), 1411–1419.

Cicconi, F., Lazic, V., Palucci, A., Almeida Assis, A. C., Romolo, F., S. 2020. Forensic Analysis of Commercial Inks by Laser-Induced Breakdown Spectroscopy (LIBS). Sensors, 20(13), 3744.

Cremers, D. A., Radziemski, L. 2006. Handbook of Laser-Induced Breakdown Spectroscopy. England: John Wiley& Sons. Inc.

Cremers, D., Radziemski, L. 2006. History and fundamentals of LIBS. In A. Miziolek, V. Palleschi, & I. Schechter (Eds.), Laser Induced Breakdown Spectroscopy (pp. 1-39). Cambridge: Cambridge University Press.

Cremers, D.A., and L.J. Radziemski. 1985. Direct detection of beryllium on filters using the laser spark. Applied spectroscopy. 39:57-63.

Effenberger, A., Scott, J. 2010. Effect of Atmospheric Conditions on LIBS Spectra. Sensors, 10(5), 4907–4925.

Elhamdaoui, I., Mohamed, N., Selmani, S., Bouchard, P., Sabsabi, M., Constantin M., Vidal F. 2022. Rapid quantitative analysis of palladium in ores using laser-induced breakdown spectroscopy assisted with laser-induced fluorescence (LIBS-LIF). Journal of Analytical Atomic Spectrometry, 37, 2537.

Fels, J., Scharner, B., Zarbock, R., Zavala Guevara, I. P., Lee, W.-K., Barbier, O. C., Thévenod, F. 2019. Cadmium complexed with β2-microglubulin, albumin and lipocalin-2 rather than metallothionein cause megalin:cubilin dependent toxicity of the renal proximal tubule. International Journal of Molecular Sciences, 20(10), 2379.

Fenelon, M. A., Hickey, R. M., Buggy, A., McCarthy, N., Murphy, E. G. 2019. Whey proteins in infant formula. Whey Proteins, 439–494.

Gajarska, Z., Brunnbauer, L., Lohninger, H., Limbeck A. 2021. Identification of 20 polymer types by means of laser-induced breakdown spectroscopy (LIBS) and chemometrics. Analytical and Bioanalytical Chemistry, 413, 6581–6594.

Genchi, G., Sinicropi, M. S., Lauria, G., Carocci, A., Catalano, A. 2020. The Effects of Cadmium Toxicity. International Journal of Environmental Research and Public Health, 17(11), 3782.

Gondal, M. A., Aldakheel, R. K., Almessiere, M. A., Nasr, M. M., Almusairii, J. A., Gondal, B. 2020. Determination of heavy metals in cancerous and healthy colon tissues using laser induced breakdown spectroscopy and its cross-validation with ICP-AES method. Journal of Pharmaceutical and Biomedical Analysis, 183, 113153

Grassi, G., Simonetti, A., Gambacorta, E., Perna, A. 2023. Effect of species on the distribution and oxidative stability of milk added of lead and cadmium, Italian Journal of Animal Science, 22:1, 1162-1171.

Guo, M., Wang, G. 2016. Milk protein polymer and its application in environmentally safe adhesives. Polymers, 8(9), 324.

Harun, H. A., Zainal, R. 2018. Laser-induced breakdown spectroscopy measurement for liquids: Experimental configurations and sample preparations. Journal of Nonlinear Optical Physics & Materials, 27(02), 1850023.

Hazra, M., Dolai, T., Giri, S., Patra, A., Dey, S. K. 2017. Synthesis of biologically active cadmium (II) complex with tridentate N_2O donor Schiff base: DFT study, binding mechanism of serum albumins (bovine, human) and fluorescent nanowires. Journal of Saudi Chemical Society, 21, S445–S456.

Hussain, S. K., Iqbal, J., Ahmad, P., Khandaker, M. U., Haq, S., Naeem, M. 2019. Laser induced breakdown spectroscopy methods and applications: A comprehensive review. Radiation Physics and Chemistry, 108666.

Janovszky, P., Kéri, A., Palásti, D., J., Brunnbauer, L., Domoki, F., Limbeck A., Galbács G. 2023. Quantitative elemental mapping of biological tissues by laser-induced breakdown spectroscopy using matrix recognition. Scientific Reports, 13, 10089.

Jaswal, B. B. S., Singh, V. K. 2015. Analytical Assessments of Gallstones and Urinary Stones: A Comprehensive Review of the Development from Laser to LIBS. Applied Spectroscopy Reviews, 50(6), 473–498.

Kaplan, D., Yalçın, Ş., H. 2022. Effect of silicon nitride coating thickness on silicon wafer substrates for signal enhancement in laser-induced breakdown spectroscopic analysis of liquids. Spectrochimica Acta Part B: Atomic Spectroscopy, 194, 106472.

Kaya, İ. 2015. Identification and detection of cis-platin binding proteins by laser induced breakdown spectroscopy [Master's thesis, İzmir Institute of Technology] https://hdl.handle.net/11147/4553.

Khan, M. R., Haq, S.U., Abbas, Q., Nadeem, A. 2022. Improvement in signal sensitivity and repeatability using copper nanoparticle-enhanced laser-induced breakdown spectroscopy. Spectrochimica Acta Part B: Atomic Spectroscopy. 195 106507.

Kilara, A., Vaghela, M., N. 2018. Whey proteins. Proteins in Food Processing, 93–126.

Kiss, K., Šindelářová, A., Krbal, L., Stejskal, V., Mrázová, K., Vrábel, J., Kaška, M., Modlitbová, P., Pořízka, P., Kaiser, J. 2021. Imaging margins of skin tumors using laser-induced breakdown spectroscopy and machine learning. Journal of Analytical Atomic Spectrometry, 36(5), 909–916.

Kurowska, E., Bal, W. 2010. Recent Advances in Molecular Toxicology of Cadmium and Nickel. Advances in Molecular Toxicology, 85–126.

Leischner, C., Egert, S., Burkard, M., Venturelli, S. 2021. Potential protective protein components of cow’s milk against certain tumor entities. Nutrients, 13(6):1974.

Lin, Q., Han, X., Wang, J., Wei, Z., Liu, K., Duan, Y. 2016. Ultra-trace metallic element detection in liquid samples using laser induced breakdown spectroscopy based on matrix conversion and crosslinked PVA polymer membrane. Journal of Analytical Atomic Spectrometry, 31(8), 1622–1630.

Liu, Y., Chen, M., Jiang, L., Song, L. 2014. New insight into molecular interaction of heavy metal pollutant-cadmium(II) with human serum albumin. Environmental Science and Pollution Research, 21(11), 6994–7005.

Liu, X., Lin, Q., Tian, Y., Liao, W., Yang, T., Qian, C., Zhang, T., Duan, Y. 2020. Metal-chelate induced nanoparticles aggregation enhances laser-induced breakdown spectroscopy for ultra-sensitive detection of trace metal ions in liquid samples. Journal of Analytical Atomic Spectrometry, 35, 188.

Ma, M., Fang, L., Zhao, N., Huang, X., Meng, D., Pan, C., Liu, J., Liu W. 2022. Simultaneous detection of heavy metals in solutions by electrodeposition assisted laser induced breakdown spectroscopy. Journal of Laser Applications, 34 (1): 012021.

Ma, S., Tang, Y., Ma, Y., Chu, Y., Chen, F., Hu, Z., Zhu, Z., Guo, L., Zeng, X., Lu Y. 2019. Determination of trace heavy metal elements in aqueous solution using surface-enhanced laser-induced breakdown spectroscopy. Optics Express, 27, 10, 15091-15099.

Ma, S., Tang, Y., Ma, Y., Dong, D., Guo, L., Zhu, H., Liu, J., Lu, Y.-F. 2019. The pH effect on the detection of heavy metals in wastewater by laser-induced breakdown spectroscopy assisted with phase transformation method. Journal of Analytical Atomic Spectrometry, 35, 198

Madureira, A. R., Pereira, C. I., Gomes, A. M. P., Pintado, M. E., Xavier Malcata, F. 2007. Bovine whey proteins – Overview on their main biological properties. Food Research International, 40(10), 1197–1211.

Markushin, Y., Sivakumar, P., Connolly, D., Melikechi, N., 2015. Tag-femtosecond laser-induced breakdown spectroscopy for the sensitive detection of cancer antigen 125 in blood plasma. Analytical and Bioanalytical Chemistry, 407, 1849–1855

Menegatti, C. R., Nicolodelli, G., Senesi, G. S., da Silva, O. A., Filho, H. J. I., Villas-Boas, P. R., Marangoni, B., S., Milori, D. M. B. P. 2019. Evaluation of LIBS under controlled atmosphere to quantify cadmium at low concentration in landfill leachates. Applied Physics B, 125(5).

Meng, Y., Gao, C., Lin, Z., Hang, W., Huang, B. 2020. Nanoscale laser-induced breakdown spectroscopy imaging reveals chemical distribution with subcellular resolution. Nanoscale Advances, 2, 3983.

Mi, Z., Wang, S., Ma, X., Zhang, Y., Liang, Y., Chen, F., Zhang, L., Wang, G., Zhang, W., Liu, Z., Luo, X., Ye, Z., Zhu, Z., Yin W., Jiaab, A. 2023. Study on direct identification of bacteria by laser-induced breakdown spectroscopy. Analytical Methods, 15, 297-303.

Musazzi, S., Perini, U. 2014. Laser-Induced Breakdown Spectroscopy Theory and Applications. Springer Series and Optical Sciences. 182.

Mutlu, N., Çiftçi, S., Gülecen, T., Öztoprak, B., G., Demir A. 2016. Laser-induced breakdown spectroscopy is a reliable method for urinary stone analysis. Turkish Journal of Urology, 42(1):21-6.

Nakanishi, R., Ohba, H., Saeki, M., Wakaida, I., Yamagishi, R.-T., Ito, Y., 2021. Highly sensitive detection of sodium in aqueous solutions using laser-induced breakdown spectroscopy with liquid sheet jets, Optics Express, 29, 5205-5212.

Niu, S., Zheng, L., Khan, A. Q., Feng, G., Zeng, H. 2018. Laser-induced breakdown spectroscopic detection of trace level heavy metal in solutions on a laser-pretreated metallic target. Talanta, 179, 312–317.

Oztoprak, B. G., Gonzalez, J., Yoo, J., Gulecen, T., Mutlu, N., Russo, R. E., Gundogdu, O., Demir, A. 2012. Analysis and classification of heterogeneous kidney stones using Laser-Induced Breakdown Spectroscopy (LIBS). Applied Spectroscopy, 66(11), 1353–1361.

O'Mahony, J. A., Fox, P. F. 2014. Milk: An Overview. Milk Proteins, 19–73.

Permyakov, E. A. 2020. α-Lactalbumin, amazing calcium-binding protein. Biomolecules, 10(9), 1210.

Pořízka, P., Klus, J., Prochazka, D., Vítková, G., Brada, M., Novotný, J., Novotný, K., Kaiser, J. 2016. Assessment of the most effective part of echelle laser-induced plasma spectra for further classification using Czerny-Turner spectrometer. Spectrochimica Acta Part B: Atomic Spectroscopy, 124, 116–123.

Rahimzadeh, R., M., Rahimzadeh, R., M., Kazemi S, Moghadamnia, A., A. 2017. Cadmium toxicity and treatment: An update. Caspian Journal of Internal Medicine, 8(3):135-145.

Rodzik, A., Pomastowski, P., Sagandykova, G.,N., Buszewski, B. 2020. Interactions of whey proteins with metal ions. International Journal of Molecular Sciences, 21(6): 2156.

Roldán, A. M., Dwivedi, V., Terreros, J. Y. S. de los, Veis, P. 2020. Laser-Induced breakdown spectroscopy (LIBS) for the analyses of faunal bones: Assembling of individuals and elemental quantification. Optik, 164992.

Ruiz, F. J., Ripoll, L., Hidalgo, M., Canals, A. 2019. Dispersive micro solid-phase extraction (DμSPE) with graphene oxide as adsorbent for sensitive elemental analysis of aqueous samples by laser induced breakdown spectroscopy (LIBS). Talanta, 191, 162-170.

Seto, T., Koga, K., Akinaga, H., Takano, F., Orii, T., Hirasawa, M. 2005. Laser ablation synthesis of monodispersed magnetic alloy nanoparticles. Journal of Nanoparticle Research, 8(3-4), 371–378.

Singh, V. K., Sharma, J., Pathak, A. K., Ghany, C. T., Gondal, M. A. 2018. Laser-induced breakdown spectroscopy (LIBS): a novel technology for identifying microbes causing infectious diseases. Biophysical reviews, 10(5), 1221–1239.

Skoog, D., A., Holler, F., J., Crouch, S., R. 2007. Instrumental analysis. Brooks/Cole, Cengage Learning.

Sobral, H., Sanginés, R., Trujillo-Vázquez, A. 2012. Detection of trace elements in ice and water by laser-induced breakdown spectroscopy. Spectrochimica Acta Part B: Atomic Spectroscopy, 78, 62–66.

Sun, L., Yu, H., Cong, Z., Xin, Y., Li, Y., Qi, L. 2015. In situ analysis of steel melt by double-pulse laser-induced breakdown spectroscopy with a Cassegrain telescope. Spectrochimica Acta Part B: Atomic Spectroscopy, 112, 40–48.

Tan, M. M., Cui, S., Yoo, J., Han, S.-H., Ham, K.-S., Nam, S.-H., Lee, Y. 2012. Feasibility of Laser-Induced Breakdown Spectroscopy (LIBS) for Classification of Sea Salts. Applied Spectroscopy, 66(3), 262–271.

Tamás, M. J., Fauvet, B., Christen, P., Goloubinoff, P. 2018. Misfolding and aggregation of nascent proteins: a novel mode of toxic cadmium action in vivo. Current genetics, 64(1), 177–181.

Tian, H., Jiao, L., Dong, D. 2019. Rapid determination of trace cadmium in drinking water using laser-induced breakdown spectroscopy coupled with chelating resin enrichment. Scientific Reports, 9(1).

Tiwari, P. K., Awasthi, S., Kumar, R., Anand, R. K., Rai, P. K., Rai, A. K. 2017. Rapid analysis of pharmaceutical drugs using LIBS coupled with multivariate analysis. Lasers in Medical Science, 33(2), 263–270.

Ünal S., Yalçın Ş. 2010. Development of a continuous flow hydride generation laser-induced breakdown spectroscopic system: determination of tin in aqueous environments. Spectrochimica Acta Part B: 65:750–757.

Wang, Y., Bu, Y., Yang, B., Cai, Y. 2023. Fastly determined electrolyte elements in human blood plasma using surface-enhanced laser-induced breakdown spectroscopy combined with a gel film method. Journal of Analytical Atomic Spectrometry, 38, 1469-1477.

Xiu, J., Gao, Q., Liu, S., Qin, H. 2020. Quantitative analysis of trace metals in aqueous solutions by laser induced breakdown spectroscopy combined with filter paper assisted analyte enrichment. Journal of Applied Spectroscopy, 87(4), 629–635.

anXue, B., Tian, Y., Li, N., Li, Q., Lu, Y., Zheng, R. 2020. Spatiotemporal and spectroscopic investigations of the secondary plasma generated during double-pulse laser-induced breakdown in bulk water. Journal of Analytical Atomic Spectrometry, 35, 2880-2892.

You, Z., Li, X., Huang, J., Chen, R., Peng, J., Kong, W., Liu, F. 2023. Agarose film-based liquid–solid conversion for heavy metal detection of water samples by Laser-Induced Breakdown Spectroscopy. Molecules, 28(6), 2777.

Zhang, D., Chen, A., Wang, Q., Zhang, H., li, S., Jin, M. 2021. Improvement of LIBS signal stability for NaCl solution using femtosecond laser-induced water film. Optics Express, 29, 9897-9906.

Zhang, S., Hu, Z., Zhao, Z., Chen, F., Tang, Y., Sheng, Z., Zhang, D., Zhang, Z., Jin, H., Pu, H., Guo, L. 2021. Quantitative analysis of mineral elements in hair and nails using calibration-free laser-induced breakdown spectroscopy. Optik, 242, 167067.

Zhang, Y., Zhang, T., Li, H. 2021. Application of laser-induced breakdown spectroscopy (LIBS) in environmental monitoring. Spectrochimica Acta Part B: Atomic Spectroscopy, 181, 106218.

Zhang Y, Li W, Duan W, Huang Z, Yang H. 2022. Echelle grating spectroscopic technology for highdouble resolution and broadband spectral measurement. Applied Sciences, 12(21):11042.

Zhu, Y., Deng, N., Hu, Z., Wang, W., Lau, C., Liu, Y., Guo L. 2022. Droplet constraint by a superhydrophobic–superhydrophilic hybrid surface with a SiO_2 NP coating for determination of heavy metals using LIBS. ACS Applied Nano Materials, 5 (12), 17508-17515.